Selective impairment of long-term depression in accumbal D1-MSNs involves calcium-permeable AMPARs in Alzheimer's disease

Nicolas Riffo-Lepe[1], Juliana Gonzalez-Sanmiguel[1], Isaías Meza[1], Paulina Saavedra-Sieyes[1], Lorena Armijo-Weingart[1,3], Armando Salinas[5], Loreto San Martín[1,2,4] & Luis G. Aguayo[1,2]*

* Corresponding author

1. Laboratorio de Neurofisiología, Departamento de Fisiología, Universidad de Concepción, Concepción, Chile

2. Programa de Neurociencia, Psiquiatría y Salud Mental (NEPSAM), Universidad de Concepción, Concepción, Chile

3. Facultad de Odontología, Universidad San Sebastián, Concepción, Chile.

4. Present address: Departamento de Bioquímica Clínica e Inmunología, Facultad de Farmacia, Concepción, Chile

5. Department of Pharmacology, Toxicology & Neuroscience, Louisiana State University Health Shreveport, Shreveport, LA, USA

Sugested reviewers:

- Marina E. Wolf, Professor of Behavioral Neuroscience, (OHSU)
- Rakez Kayed, University of Texas Medical Branch (UTMB)
- Marcello D'Amelio, Medical School University Campus Bio-medico
- Marco Fuenzalida, Universidad de Valparaíso

Abstract

Early neuropsychiatric symptoms in Alzheimer's disease emerge before cognitive decline, yet their synaptic basis remains poorly defined. Here we identify an early, cell-type-specific disruption of synaptic plasticity in the nucleus accumbens during pre-plaque stages of disease. In APP/PS1 mice, intracellular amyloid-beta accumulation is associated with a selective loss of mGluR1/5-dependent long-term depression in dopamine D1 receptor–expressing medium spiny neurons, despite comparable intracellular amyloid-beta levels across neuronal subtypes. This impairment is accompanied by aberrant postsynaptic remodeling characterized by functional accumulation of calcium-permeable AMPA receptors and increased excitatory drive. These synaptic alterations coincide with reduced dopamine-dependent signaling and selective changes in reward-related behavior, including altered hedonic consumption. Together, these findings identify an early vulnerability of the mesolimbic reward system and suggest that non-cognitive manifestations of Alzheimer's disease arise from circuit-level imbalance before plaque deposition.

Introduction

Alzheimer's disease (AD) is the most prevalent form of dementia, resulting from the complex interplay between genetic susceptibility and environmental factors that range from mutations in genes critical for neuronal function to social and lifestyle factors [1, 2]. Although memory impairments have long been considered the primary clinical hallmark of AD [3], new evidence indicates that neuropsychiatric symptoms such as mood disturbances, motivational deficits, and compulsive behaviors show up before cognitive decline and strongly predict later dementia [4, 5]. Despite their relevance, the cellular and

circuit-level mechanisms underlying these early non-cognitive alterations remain poorly understood, particularly within subcortical regions implicated in emotional and motivational regulation [6].

A key feature of AD progression is the temporal progression between intracellular and extracellular amyloid-beta (Aβ) pathology. While extracellular Aβ plaques appear at advanced disease stages in humans and animal models, intracellular Aβ accumulation occurs months to years earlier, and is now recognized as one of the earliest pathological events, preceding extracellular Aβ plaque and neurofibrillary tangle deposition [6-11]. Intracellular Aβ disrupts calcium signaling, synaptic homeostasis, and neuronal excitability [11-13], yet the consequences of this pathology outside canonical hippocampal and cortical circuits remain largely unexplored.

Emerging evidence indicates that early pathological changes also affect the mesolimbic system [14-16]. The nucleus accumbens (nAc), a central integrative hub within this circuit, receives convergent glutamatergic inputs from the prefrontal cortex, amygdala, hippocampal subiculum, and thalamus, and dopaminergic projections from the ventral tegmental area (VTA) [17]. Through these connections, the nAc integrates motivational, affective, and cognitive signals that are essential for reward processing, goal-directed behavior, and social interaction [17, 18]. Notably, accumulating evidence from patients and mouse models indicates that nAc dysfunction precedes cognitive decline, suggesting that early alterations in mesolimbic signaling contribute to the emergence of non-cognitive symptoms in AD [16, 19-22]. In this context, we previously reported intracellular Aβ accumulation accompanied by increased neuronal excitability in the nAc of 6-month-old APP/PS1 mice, in the absence of extracellular plaque deposition [21], raising the

possibility that intracellular Aβ disrupts synaptic physiology in the nAc during early stages of the disease.

Medium spiny neurons (MSNs), the principal neuronal type in the nAc, coordinate information flow via dopamine receptor type 1 (D1R)- and dopamine receptor type 2 (D2R)-expressing pathways [17, 23]. Balanced excitation and inhibition within these pathways are essential for emotional regulation and motivational salience [24, 25]. Long-term depression (LTD) represents the predominant form of enduring synaptic plasticity in the nAc and functions as a key mechanism for constraining excitatory drive, thereby preventing pathological strengthening of glutamatergic inputs [26, 27]. Accumbal LTD critically depends on AMPA receptor (AMPAR) remodeling driven by the group I metabotropic glutamate receptor (mGluR1/5) signaling, which promotes the endocytosis of calcium-permeable AMPARs (CP-AMPARs) to maintain synaptic homeostasis [28, 29]. Disruption of this LTD mechanism favors the synaptic accumulation of CP-AMPARs in the nAc, enhances excitatory transmission, and reinforces direct pathway output, as demonstrated in addiction and food-restriction paradigms [30-37].

AMPARs are tetrameric ionotropic receptors composed of GluA1–4 subunits that mediate fast excitatory transmission in the brain [38]. Their calcium permeability depends on the presence or absence of the GluA2 subunit, which undergoes RNA editing at the Q/R site to render AMPARs calcium-impermeable [39]. AMPA receptors lacking edited GluA2 and GluA1 homomers are calcium-permeable, show inward rectification currents, and contribute to forms of plasticity involving rapid AMPAR trafficking [38, 39]. Although CP-AMPARs have been implicated in various pathological conditions, including

addiction, eating disorders, and stress [37, 40, 41], their regulation in the nAc during early AD remains unknown.

Within this framework, two key questions remain unresolved. First, does intracellular Aβ alter AMPAR composition or LTD mechanisms in the nAc during early disease stages, prior to plaque deposition? Second, are specific MSN subtypes differentially vulnerable to these alterations? Although intracellular Aβ oligomers disrupt AMPAR trafficking and synaptic function in hippocampal neurons [42], it remains unknown whether similar mechanisms operate in accumbal MSNs. Moreover, it is unclear whether D1R- and D2R-expressing pathways are differentially affected during early stages of the disease. Notably, no study to date has examined how intracellular Aβ accumulation influences LTD or AMPAR function in distinct MSN subtypes during the earliest phases of AD progression.

Recent evidence indicates that dopaminergic dysfunction is an early event in AD, preceding cognitive impairment [43]. Reduced dopamine levels, degeneration of VTA dopaminergic neurons, and decreased dopamine transporter expression in the nAc have been reported in patients and AD mouse models [16, 44-46]. Collectively, these observations highlight a potential convergence between early dopaminergic dysfunction in the mesolimbic system and synaptic plasticity impairments emerging during initial stages of Aβ pathology. However, whether intracellular Aβ contributes to synaptic dysfunction in accumbal MSNs during early AD remains unknown. Here, we hypothesized that intracellular Aβ disrupts postsynaptic homeostasis in D1R-positive MSNs, leading to aberrant plasticity and excitatory imbalance that may underlie early motivational and affective alterations associated with AD. Elucidating these

mechanisms provides insight into the synaptic basis of early non-cognitive symptoms and may inform the identification of molecular targets for early-stage therapeutic intervention.

RESULTS

Intracellular Aβ accumulates broadly in accumbal MSNs during early stages of APP/PS1 pathology.

To establish the temporal onset of amyloid pathology in the nucleus accumbens during early Alzheimer's disease progression, we first performed immunohistochemistry in coronal sections from WT and APP/PS1 mice at 3 months of age using the MoAβ2 antibody, which recognizes the N-terminal region of Aβ without cross-reacting with APP. At this age, intracellular Aβ signal was detected within neuronal somata, with no evidence of extracellular plaque deposition, consistent with our previous observations at 6 months. Quantitative analysis revealed a significant increase in intracellular Aβ signal in APP/PS1 compared with WT mice, indicating that accumbal neurons already accumulate Aβ intracellularly at very early stages of disease progression (Fig. 1A, B).

To determine whether this intracellular Aβ accumulation is differentially distributed across MSN subtypes at later pre-plaque stages, we next analyzed 6-month-old WT/D1RtdT and APP/PS1/D1RtdT mice. Consistent with our previous report in 6-month-old APP/PS1 mice[21], APP/PS1/D1RtdTomato animals exhibited robust intracellular Aβ accumulation restricted to neuronal somata in the nucleus accumbens, with no detectable extracellular plaques (Fig. 1C). Quantitative analysis revealed a significant increase in Aβ intensity in both D1R+ and D1R− MSNs compared with WT

controls (Fig. 1D), indicating that intracellular Aβ accumulation during pre-plaque stages occurs broadly across MSN subtypes rather than selectively targeting a specific neuronal population.

To anchor these findings within the broader progression of amyloid pathology, we evaluated extracellular plaque deposition using Thioflavin-S staining in coronal brain sections from WT and APP/PS1 mice at 6 and 12 months of age (Fig. S1A). No plaques were detected in the nAc at 6 months, whereas sparse plaques appeared at 12 months. In contrast, amyloid plaques were readily detected in the cortex of APP/PS1 mice at both ages (Fig. S1B). Together, these data indicate that amyloid pathology in the nAc is predominantly intracellular during early disease stages, preceding extracellular plaque formation.

Finally, to evaluate whether early intracellular Aβ accumulation is associated with inflammatory responses, we quantified Iba1+ microglia in the nAc of 6-month-old WT and APP/PS1 mice. No differences in Iba1+ cell number or fluorescence intensity were detected between genotypes, indicating the absence of overt microglial activation at this stage (Fig. S1C, D). Together, these results show that intracellular Aβ accumulates in both D1R+ and D1R− MSNs in the nAc during pre-plaque stages, defining an early histopathological window preceding extracellular aggregation.

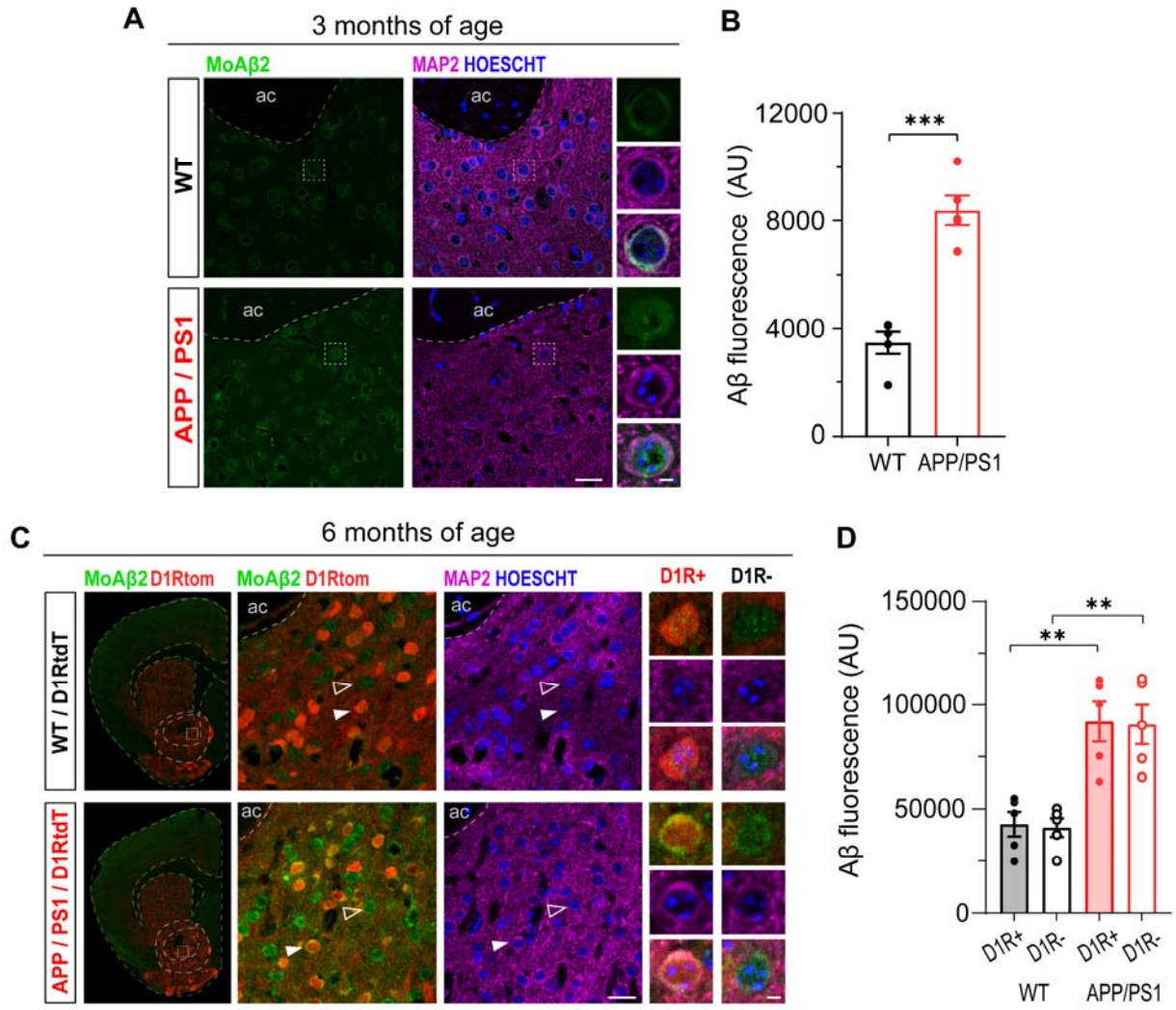

Fig. 1 | Intracellular Aβ accumulates in both D1R+ and D1R− MSNs in the nAc of APP/PS1 mice during pre-plaque stages. A Representative immunohistochemistry of coronal nAc sections (30 µm) from 3-month-old WT and APP/PS1 mice labeled with MOAβ-2, MAP2, and Hoechst. APP/PS1 mice show detectable intracellular Aβ immunoreactivity. Right panels display magnified insets (dashed boxes) highlighting intracellular signal within individual neuronal somata. **B** Quantification of MOAβ-2 fluorescence intensity under a MAP2 mask shows significantly higher intracellular Aβ levels in APP/PS1 mice compared with WT (unpaired two-tailed t test, t(8)=7.111,

p<0.001). Each point represents the mean value per animal (WT n=5; APP/PS1 n=5). A total of 20 neurons per animal were analyzed. **C Immunohistochemistry of 6-month-old WT/D1RtdTomato and APP/PS1/D1RtdTomato nAc sections labeled with MOAβ-2, D1RtdTomato, MAP2, and Hoechst. Left panels show tile-scan images; middle panels present magnified fields (dashed boxes). Filled white arrowheads indicate D1R+ MSNs (tdTomato+), whereas open white arrowheads denote D1R− MSNs (tdTomato−). Right panels show single-cell zoom-ins corresponding to each MSN subtype **D** Quantification of intracellular Aβ intensity in identified D1R+ and D1R− MSNs at 6 months. APP/PS1 mice exhibit significantly elevated Aβ levels in both MSN subtypes compared with WT (one-way ANOVA followed by Tukey's test: WT D1R+ vs WT D1R−, ns; WT D1R+ vs APP/PS1 D1R+, p=0.002; WT D1R+ vs APP/PS1 D1R−, p=0.002; WT D1R− vs APP/PS1 D1R+, p=0.001; WT D1R− vs APP/PS1 D1R−, p=0.002; APP/PS1 D1R+ vs APP/PS1 D1R−, ns). Each point represents the mean value per animal (n=5 per genotype). A total of WT: 50 D1R+ and 47 D1R− cells, APP/PS1: 40 D1R+ and 35 D1R− cells were analyzed. Scale bars: 20 µm; insets scale bar 5 µm

Selective impairment of long-term depression in D1R+ MSNs of the nAc in early-stage APP/PS1 mice.

To determine whether intracellular Aβ accumulation disrupts accumbal synaptic plasticity, we used electrophysiology in accumbal brain slices of 3- and 6-month-old WT and APP/PS1 mice. LTD was induced by a high frequency stimulation (HFS) protocol in presence of NMDARs and GABAARs blockers, 2-amino-5-phosphonovaleric acid (APV) and Picrotoxin (PTX) respectively, isolating electrically evoked excitatory postsynaptic currents (eEPSCs) mediated mostly by AMPARs. At 3-months-old, HFS-LTD was

184 robust and similar between WT and APP/PS1 mice (WT: ~40%; APP/PS1: ~40%; p =
185 0.6849). In contrast, at 6 months, LTD was markedly reduced in APP/PS1 mice (47.3 ±
186 3.2% in WT vs. 11.4 ± 4.0% in APP/PS1; $t(16) = 3.386$, $p = 0.0038$, $\eta^2 = 0.4174$) (Fig
187 2S. A-G), indicating loss of HFS-LTD at 6 but normal at 3 months old, supporting the
188 idea of a progressive dysregulation of accumbal synaptic plasticity at early AD stages.

189 We next evaluated mGluR-dependent LTD using the bath application of the mGluR(1/5)
190 agonist, (RS)-3,5-Dihydroxyphenylglycine (DHPG) (50 µM). Quantitative analysis
191 revealed a marked reduction in mGluR-LTD magnitude in APP/PS1 accumbal slices
192 compared with WT controls. An unpaired two-tailed t-test showed a significant
193 difference between genotypes ($t(13) = 4.155$, $p = 0.0011$), with WT neurons exhibiting
194 robust LTD (35.33%) whereas APP/PS1 neurons displayed a strongly attenuated
195 response (11.45%) (Fig. 2S, H–K). These findings indicate that, in addition to impaired
196 HFS-induced LTD, mGluR-LTD is also significantly disrupted at 6 months of age in
197 APP/PS1 mice. Notably, since picrotoxin (PTX) (100 µM) and the NMDAR antagonist
198 APV (50 µM) were present on the bath solution, these results suggest that neither
199 $GABA_A$Rs, GlyRs nor NMDARs are involved in the LTD impairment.

200 To assess cell-type specificity, we recorded evoked EPSCs before and after LTD
201 induction and evaluated paired-pulse responses in D1R+ and D1R− MSNs from 6-
202 month-old WT/D1RtdTomato and APP/PS1/D1RtdTomato mice, in which tdTomato
203 selectively labels D1R-expressing neurons (Fig. 2A). HFS-LTD was significantly
204 reduced in APP/PS1 D1R+ MSNs compared with WT D1R+ MSNs (Fig. 2B,C; one-way
205 ANOVA, $F(3,19) = 6.170$, $p = 0.004$; Tukey, $p = 0.015$), whereas D1R− MSNs displayed
206 preserved LTD across genotypes and differed significantly from APP/PS1 D1R+ MSNs

(p = 0.005; Fig. 2D). Paired-pulse ratio was unchanged between groups (Fig. 2E), indicating intact presynaptic release probability. Together, these results demonstrate a selective postsynaptic loss of HFS-LTD in accumbal D1R+ MSNs during early AD stages.

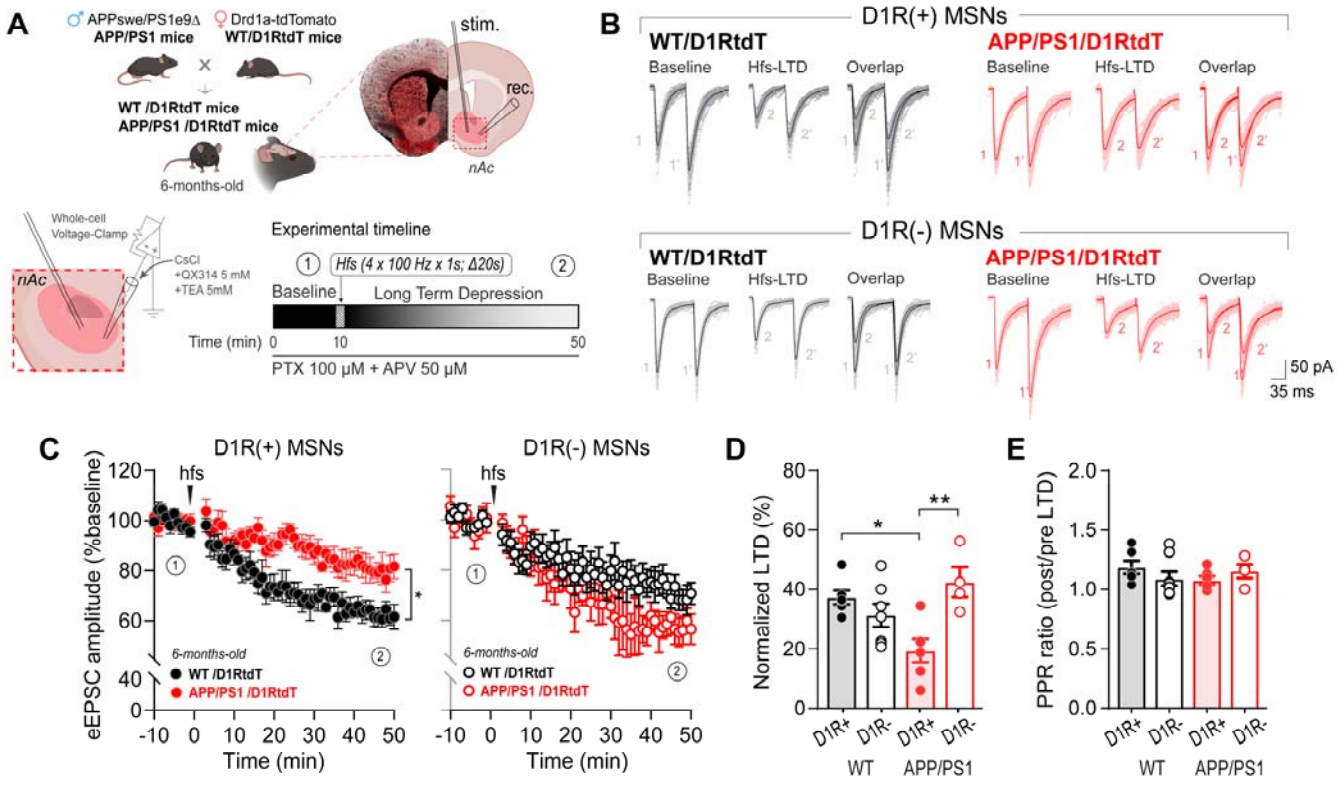

Fig. 2 | HFS-LTD is selectively impaired in D1R+ MSNs, but preserved in D1R− MSNs, in the nAc of 6-month-old APP/PS1 mice. A Schematic representation of the experimental strategy. Crossing APP/PS1 mice with Drd1-tdTomato animals enables selective identification of D1R+ MSNs. The experimental timeline indicates baseline eEPSC acquisition (1; 10 min), HFS-LTD induction (four trains of 100 Hz, 1 s, every 20 s), and monitoring of LTD expression. LTD magnitude was calculated by normalizing the mean eEPSC amplitude measured during the final 10 min of the recording period (2; 40–50 min) to the baseline period (1). **B** Representative pair-pulse evoked EPSC traces

recorded from D1R+ and D1R− MSNs in WT/D1RtdT and APP/PS1/D1RtdT mice before (baseline) and after HFS-LTD induction. Overlaid traces illustrate changes in synaptic strength. Paired-pulse stimulation was used to assess presynaptic release probability. **C** Time course of normalized eEPSC amplitude in D1R+ (left) and D1R− (right) MSNs. A significant reduction in LTD was observed only in D1R+ MSNs of APP/PS1 mice compared with WT littermates, whereas D1R− MSNs exhibited preserved LTD. Data are shown as mean ± s.e.m. **D** Quantification of LTD magnitude calculated from the last 10 min of the recording (40–50 min) revealed a significant reduction of LTD in D1R+ MSNs from APP/PS1 mice compared with WT D1R+ MSNs (one-way ANOVA, $F(3,19)=6.170$, $p=0.004$; Tukey's post hoc test, WT D1R+ vs. APP/PS1 D1R+, $p=0.015$). In addition, LTD magnitude differed between D1R+ and D1R− MSNs within APP/PS1 mice (Tukey's post hoc test, $p=0.005$). **E** Quantification of paired-pulse ratio (PPR; post/pre) showed no significant differences between genotypes or MSN subtypes (Kruskal–Wallis test, $p=0.279$; Dunn's multiple comparisons test). Each data point represents a single recorded neuron. Number of cells and animals analyzed: WT D1R+ (n=6 cells, 5 mice), WT D1R− (n=7 cells, 5 mice), APP/PS1 D1R+ (n=6 cells, 5 mice), APP/PS1 D1R− (n=4 cells, 3 mice). Graphs show mean ± s.e.m. *$p<0.05$, **$p<0.01$.

Postsynaptic upregulation of AMPAR signaling selectively affects accumbal D1R+ MSNs in APP/PS1 mice at an early stage.

To determine whether the impairment in LTD observed in APP/PS1 mice is associated with alterations in glutamatergic synaptic transmission, we first quantified the AMPA/NMDA ratio in MSNs of the nAc. Whole-cell voltage-clamp recordings were

243 performed at a holding potential of +40 mV to relieve the Mg^{2+} block of NMDARs,
244 allowing simultaneous measurement of AMPAR- and NMDAR-mediated components,
245 followed by pharmacological isolation and digital subtraction of NMDA currents (Fig.
246 3A–B). APP/PS1 MSNs exhibited a significant reduction in the AMPA/NMDA ratio
247 compared with WT controls (Fig. 3C).
248 Because AMPAR-mediated currents recorded at depolarized potentials are strongly
249 influenced by receptor subunit composition, including inward rectification and polyamine
250 block characteristic of Ca^{2+}-permeable AMPARs [39], this reduction is unlikely to reflect a
251 generalized decrease in excitatory synaptic strength. Rather, it suggests a postsynaptic
252 reorganization of AMPAR populations and/or altered receptor surface expression.
253 To determine whether these functional changes were associated with altered synaptic
254 protein expression, we assessed pre- and postsynaptic markers in nAc tissue by
255 Western blot. Levels of the presynaptic protein SV2 were unchanged between WT and
256 APP/PS1 mice (Fig. 3D–E), indicating preserved presynaptic integrity. In contrast, the
257 postsynaptic scaffolding protein PSD95 and the AMPAR subunits GluA1 and GluA2
258 were significantly increased in APP/PS1 mice (Fig. 3D–E). These results indicate that
259 LTD impairment is associated with postsynaptic glutamatergic remodeling rather than
260 presynaptic alterations.
261 To determine whether these changes arise from transcriptional regulation, we examined
262 mRNA levels for GluA1, GluA2, Grin1, and Grin2b at 6 and 9 months of age. No
263 significant genotype differences were detected at either stage (Fig. 3S), indicating that
264 the elevated AMPAR protein levels likely result from post-transcriptional or translational
265 mechanisms rather than altered gene expression.

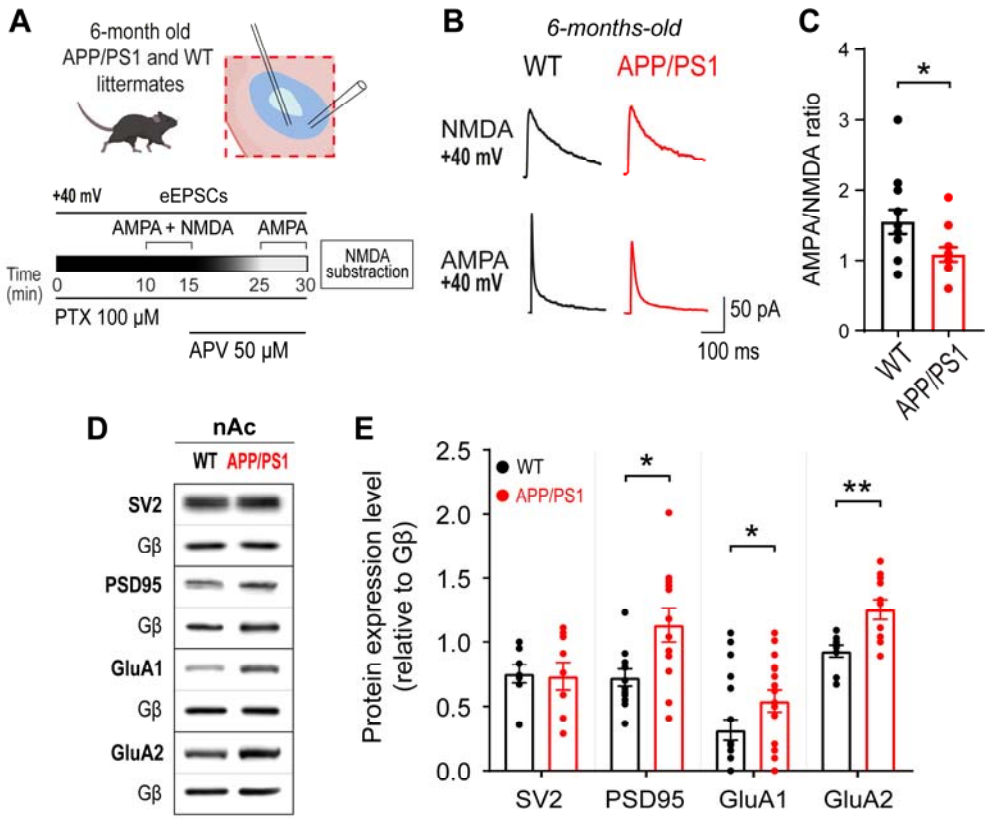

Fig. 3 | AMPAR-related synaptic alterations in the nucleus accumbens of 6-month-old APP/PS1 mice. A Schematic representation of the experimental design used to assess AMPAR- and NMDAR-mediated synaptic transmission in MSNs of the nAc from 6-month-old WT and APP/PS1 mice. Whole-cell voltage-clamp recordings were performed at +40 mV to isolate mixed AMPA+NMDA eEPSCs, followed by pharmacological isolation of AMPAR-mediated currents after APV application and digital subtraction to obtain NMDA receptor–mediated component. **B** Representative AMPAR- and NMDAR-mediated eEPSCs recorded at +40 mV from MSNs of WT (black) and APP/PS1 (red) mice, illustrating the subtraction-based isolation of NMDA currents. **C** Quantification of the AMPA/NMDA ratio reveals a significant reduction in APP/PS1 mice compared with WT (unpaired two-tailed t-test, $t(23) = 2.236$, $P = 0.027$; WT: $n = 12$

neurons, 4 mice; APP/PS1: n = 13 neurons, 4 mice). **D** Representative Western blots of synaptic proteins extracted from the nAc of WT and APP/PS1 mice. **E** Quantification of protein expression levels normalized to Gβ shows no significant difference in the presynaptic marker SV2 between genotypes, whereas postsynaptic proteins PSD95, GluA1, and GluA2 are significantly increased in APP/PS1 mice (unpaired two-tailed t-tests). Sample sizes (WT/APP/PS1): SV2, n = 8/9; PSD95, n = 12/12; GluA1, n = 22/16; GluA2, n = 9/11. Data are shown as mean ± s.e.m. *p < 0.05, **p < 0.01.

We next examined excitatory synaptic transmission at 3 and 6 months. AMPAR-mediated spontaneous EPSCs, recorded at – 60 mV in the presence of PTX and APV and blocked by CNQX, were similar between WT and APP/PS1 mice at 3 months of age (Fig. 4S, A–I). In contrast, at 6-months-old APP/PS1 MSNs exhibited increased sEPSC amplitude without changes in frequency or kinetics (Fig. 4S, J–R), accompanied by a rightward shift in cumulative amplitude distributions (Fig. 4S, L–M). Thus, despite early intracellular Aβ accumulation, functional synaptic alterations emerge at 6 months, coinciding with the onset of LTD deficits.

Finally, to determine whether these postsynaptic changes are specific to MSN subtypes, we performed whole-cell recordings in WT/D1RtdT and APP/PS1/D1RtdT mice (Fig. 4). A two-way ANOVA revealed a significant genotype × MSN-type interaction for sEPSC amplitude ($F(3,18) = 5.856$, $p = 0.0057$). Sidak's post hoc test showed a significant increase in amplitude exclusively in APP/PS1 D1R+ MSNs compared with WT D1R+ MSNs, whereas D1R− MSNs showed no genotype differences (Fig. 4C-D, G). Importantly, sEPSC frequency remained unchanged across genotypes and MSN

subtypes (Fig. 4F), supporting the conclusion that these alterations arise from postsynaptic rather than presynaptic mechanisms.

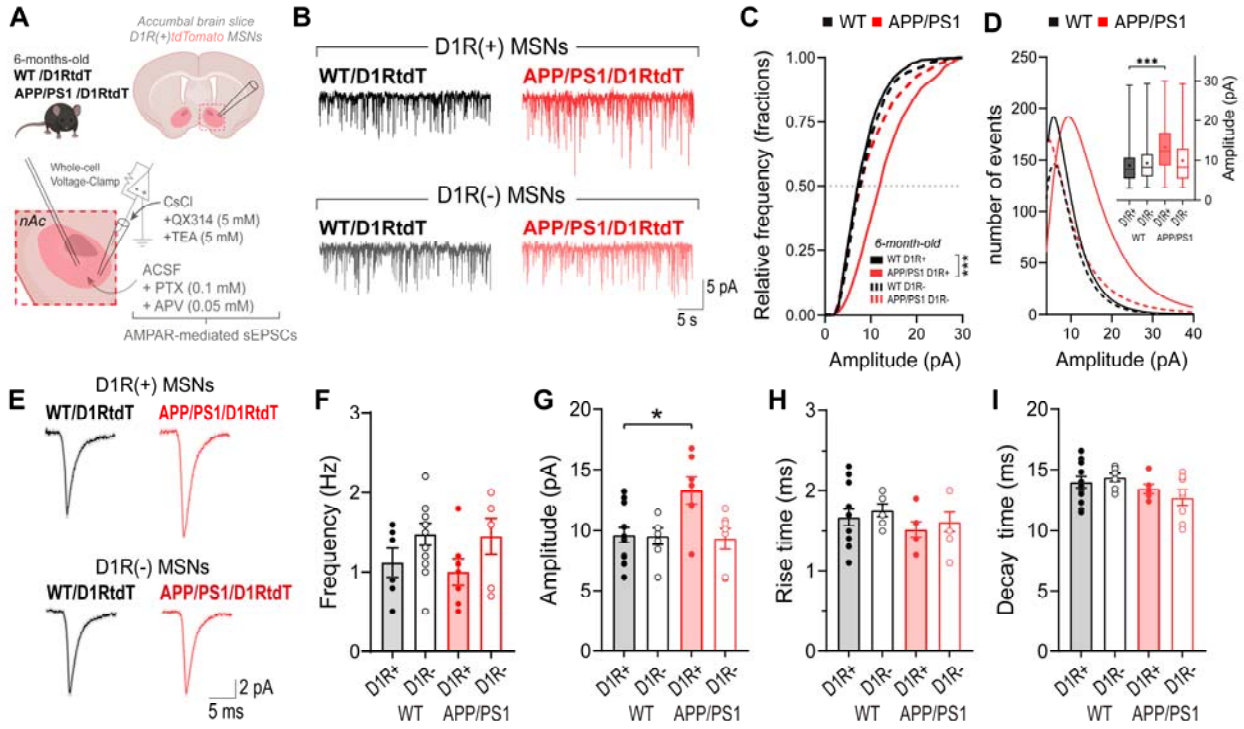

Fig. 4 | Enhanced AMPAR-mediated excitatory transmission selectively in D1R+ MSNs of 6-month-old APP/PS1 mice. A Schematic representation of the experimental configuration for whole-cell voltage-clamp recordings of AMPAR-mediated spontaneous EPSCs (sEPSCs) in nucleus accumbens slices from 6-month-old WT/D1RtdT and APP/PS1/D1RtdT mice. **B** Representative sEPSC traces recorded at −60 mV from D1R+ (top) and D1R− (bottom) MSNs in WT (black) and APP/PS1 (red) mice. **C** Cumulative probability distributions of sEPSC amplitudes showing a rightward shift selectively in APP/PS1 D1R+ MSNs compared with WT D1R+ MSNs (Welch's ANOVA, $p < 0.001$). **D** Amplitude distribution histograms and box plots reveal a significant increase in sEPSC amplitude in APP/PS1 D1R+ MSNs relative to WT D1R+ MSNs (Games–Howell post hoc test, mean difference = −4.71 pA, 95% CI −5.29 to −4.14, $p <$

0.001), whereas no difference was detected between WT and APP/PS1 D1R− MSNs ($p = 0.094$). **E** Representative averaged sEPSC event from D1R+ and D1R− MSNs in WT/D1RtdT and APP/PS1/D1RtdT mice. **F** Quantification of sEPSC frequency shows no significant differences across groups (one-way ANOVA, $F(3,27) = 1.89$, $p = 0.155$). **G** Two-way ANOVA of sEPSC amplitude reveals a significant interaction between genotype and MSN subtype ($F(1,18) = 5.86$, $p = 0.0057$). Šídák post hoc comparisons show increased sEPSC amplitude in APP/PS1 D1R+ MSNs compared with WT D1R+ MSNs (mean difference = −2.67 pA, 95% CI −5.28 to −0.07, $p = 0.044$), with no differences in D1R− MSNs ($p = 0.979$). **H** Rise time analysis shows no significant differences among groups (one-way ANOVA, $F(3,30) = 0.66$, $p = 0.582$). **I** Decay time analysis shows no significant differences among groups (one-way ANOVA, $F(3,30) = 1.88$, $p = 0.154$). Data are presented as mean ± s.e.m. *$p < 0.05$, ***$p < 0.001$.

Together, these results reveal a progressive, postsynaptic upregulation of AMPAR signaling in the nAc of APP/PS1 mice that selectively targets D1R+ MSNs. This cell-type specific strengthening of excitatory synaptic transmission aligns with the selective impairment of LTD in 6-months-old D1R+ MSNs and may contribute to altered mesolimbic function during early stages of Alzheimer's disease.

Functional upregulation of calcium-permeable AMPA receptors in the nAc of APP/PS1 mice.

Considering the postsynaptic alterations found in the APP/PS1 mice, we next asked whether these changes reflect an early shift in AMPAR subunit composition toward CP-AMPARs, which lacks the GluA2 subunit or contain non edited GluA2 subunit,

contribute to increased Ca^{2+} influx, show inward rectification, and sensitivity to selective antagonists such as NASPM [35].

To assess AMPAR-mediated Ca^{2+} signaling in the nAc, we expressed GCaMP6s in the nAc of 6-months-old WT and APP/PS1 mice and recorded electrically evoked Ca^{2+} transients in acute accumbal brain slices (Fig. 5A-D). Bath application of CNQX (5 µM) was used to estimate the AMPAR-dependent component of the Ca^{2+} response by quantifying the reduction in fluorescence following AMPAR blockade. APP/PS1 accumbal slices displayed significantly larger CNQX-sensitive reductions in Ca^{2+} transients compared with WT slices (Fig. 5C-D), indicating that a greater proportion of evoked Ca^{2+} activity depends on AMPAR activation in the nAc of APP/PS1 mice. Because GluA2-lacking AMPARs allow Ca^{2+} influx and can enhance downstream Ca^{2+} signaling, this increase is consistent with a higher calcium activity driven by AMPARs in early stages of AD in the nAc of APP/PS1 mice and points to an increase of CP-AMPARs .

We next assessed the rectification behavior associated with CP-AMPARs by quantifying the rectification index (RI) of AMPAR-mediated eEPSCs recorded at holding potentials from −60 mV to +40 mV in 20 mV steps (Fig. 5E-H). The data shows that APP/PS1 MSNs displayed markedly smaller current amplitudes at depolarized voltages compared with WT MSNs, resulting in a significantly lower RI (WT ≈ 0.7; APP/PS1 ≈ 0.4, unpaired two-tailed t-test, $t(14) = 2.989$, $p = 0.0098$) (Fig. 5H). This inward rectification property reflects voltage-dependent block of GluA2-lacking AMPARs by intracellular polyamines, enabling functional identification of CP-AMPARs [39]. Therefore, these findings provide

358 evidence for increased incorporation of calcium-permeable AMPARs at accumbal
359 synapses in APP/PS1 mice at early AD stages.

360 To directly test CP-AMPAR involvement, we applied NASPM (150 µM) while recording
361 AMPAergic eEPSCs in nAc MSNs (Fig. 5I-K). NASPM produced a larger inhibition in
362 APP/PS1 MSNs (~40% reduction) than in WT MSNs (~20%) (Fig. 5K), consistent with
363 an increased contribution of calcium-permeable, NASPM-sensitive AMPARs to synaptic
364 transmission in APP/PS1 mice in early AD.

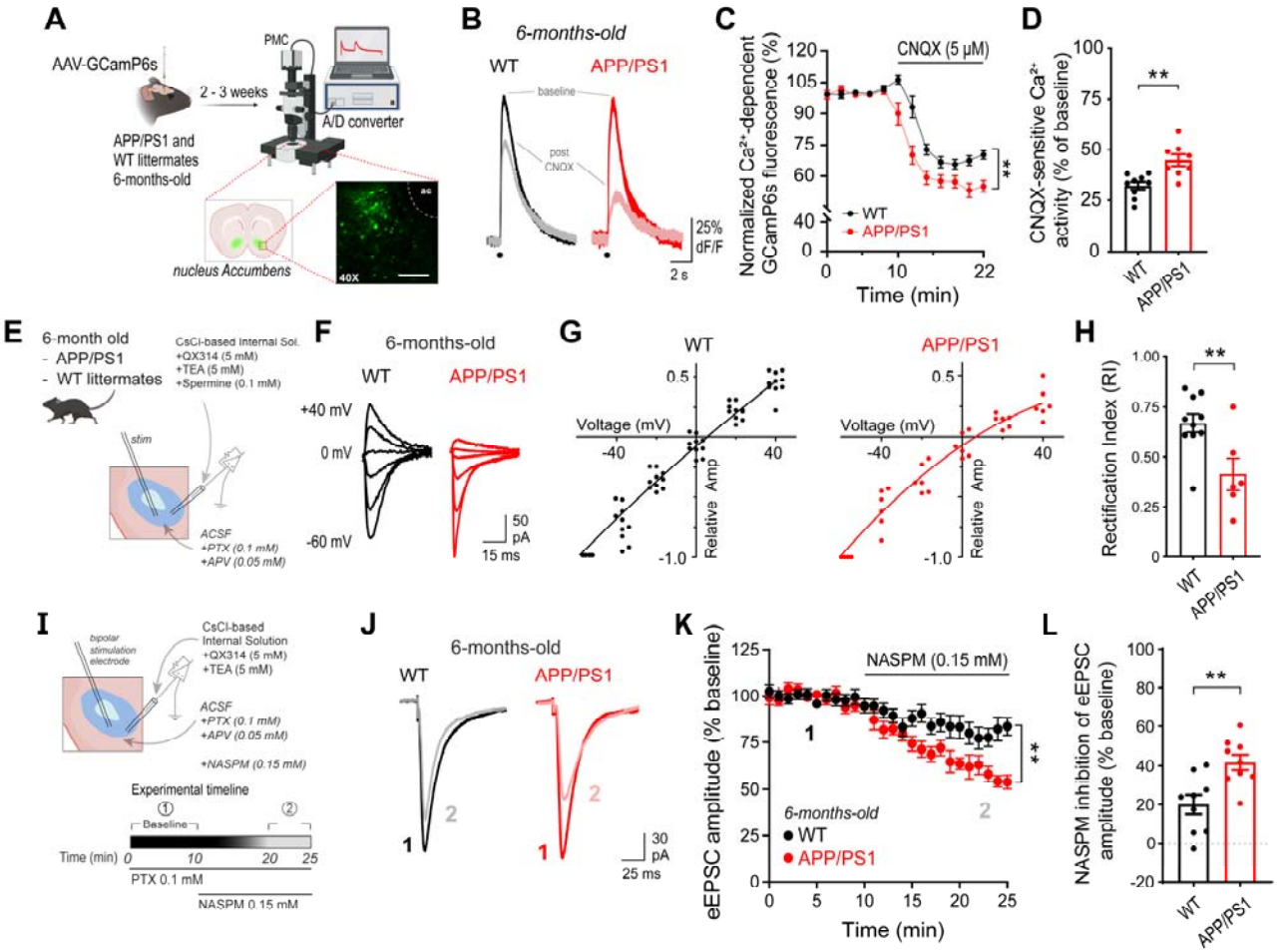

365

366 **Fig. 5 | Enhanced functional contribution of calcium-permeable AMPA receptors**
367 **in the nucleus accumbens of APP/PS1 mice at pre-plaque stages. A** AAV-

GCaMP6s was injected into the nAc of WT and APP/PS1 mice and allowed to express for 2–3 weeks before acute slice preparation for calcium imaging. **B** Representative electrically evoked calcium transients recorded in the nAc of 6-month-old WT (black) and APP/PS1 (red) mice before and after application of the AMPAR antagonist CNQX. **C** Time course of normalized GCaMP6s-dependent Ca^{2} fluorescence (% of baseline) showing a larger CNQX-induced reduction in APP/PS1 slices. **D** Quantification of CNQX-sensitive Ca^{2} activity reveals significantly greater inhibition in APP/PS1 mice compared with WT (unpaired two-tailed t-test, $t(15) = 3.725$, $p = 0.002$; WT 9 recordings/4 mice, APP/PS1 8/4). **E** Whole-cell voltage-clamp configuration for recording electrically evoked EPSCs (eEPSCs) in MSNs from the nAc of 6-month-old mice. Recordings were performed using an internal solution containing spermine (100 µM). **F** Representative eEPSC traces recorded at - 60 mV to + 40 mV (delta = 20 mV) from WT (black) and APP/PS1 (red) MSNs. **G** Current–voltage relationships showing reduced inward rectification in APP/PS1 MSNs. **H** Quantification of the RI shows a significant decrease in APP/PS1 MSNs (unpaired two-tailed t-test, $t(14) = 2.989$, $p = 0.0098$). **I** Experimental protocol for pharmacological isolation of calcium-permeable AMPARs using NASPM. **J** Representative eEPSC traces recorded before and after NASPM application (150 µM). **K** Time course of normalized eEPSC amplitude (% of baseline) showing greater NASPM-induced inhibition in APP/PS1 MSNs. **L** Quantification of NASPM-sensitive eEPSC inhibition confirms increased NASPM sensitivity in APP/PS1 MSNs compared with WT (unpaired two-tailed t-test, $t(14) = 2.98$, $p = 0.0098$). Data are presented as mean ± s.e.m.; each data point represents a single recording or neuron.

Together, these converging imaging, electrophysiological, and pharmacological results demonstrate a robust upregulation of CP-AMPARs in the nAc of APP/PS1 mice. This shift in AMPAR subunit composition provides a mechanistic basis for the enhanced excitatory transmission and impaired LTD observed in D1R+ MSNs at 6 months of age in transgenic mice, implicating the pathological incorporation of calcium-permeable AMPARs as a central contributor to accumbal dysfunction during early stages of Alzheimer's disease.

CP-AMPAR accumulation occludes mGluR-LTD selectively in D1R+ MSNs of APP/PS1 mice.

Given that APP/PS1 mice exhibit both impaired LTD and enhanced CP-AMPAR signaling in the nAc, we next examined whether the incorporation of GluA2-lacking AMPARs interferes with the expression of mGluR1/5-dependent LTD, which is reported as the principal homeostatic LTD mechanism that induce CP-AMPAR endocytosis[28]. To address this, we performed whole-cell recordings in D1R+ and D1R− MSNs from 6-month-old WT/D1RtdT and APP/PS1/D1RtdT mice using a sequential protocol consisting of baseline acquisition, induction of mGluR-LTD with DHPG (50 µM), and subsequent application of NASPM (150 µM) to block CP-AMPARs (Fig. 6A,B).

In WT D1R+ MSNs, application of DHPG induced a robust and sustained depression of eEPSC amplitude, consistent with intact mGluR1/5-LTD (Fig. 6C,D). Under these conditions, subsequent NASPM application did not produce further suppression of synaptic currents (Fig. 6C,D), indicating a minimal residual CP-AMPAR contribution after LTD induction.

In APP/PS1 D1R+ MSNs, DHPG failed to induce significant synaptic depression, indicating a selective impairment of mGluR1/5-dependent LTD (Fig. 6C). Notably, subsequent application of NASPM after DHPG produced a robust additional reduction in eEPSC amplitude, reaching levels of synaptic depression comparable to those observed in WT neurons following LTD induction (Fig. 6C,D). Analysis of the paired-pulse ratio before and after LTD induction revealed no significant differences across conditions (Fig. 6E), indicating that presynaptic release probability remained unchanged. These data demonstrate that mGluR1/5-LTD impairment in APP/PS1 D1R+ MSNs originates from postsynaptic mechanisms. Together, these findings indicate that impaired mGluR1/5-dependent LTD is associated with persistent functional incorporation of CP-AMPARs at accumbal D1R+ synapses. Importantly, selective CP-AMPAR blockade is sufficient to reinstate synaptic depression, supporting the conclusion that abnormal retention of CP-AMPARs contributes directly to the loss of LTD and enhanced excitatory transmission observed in the nAc during early APP/PS1 pathology.

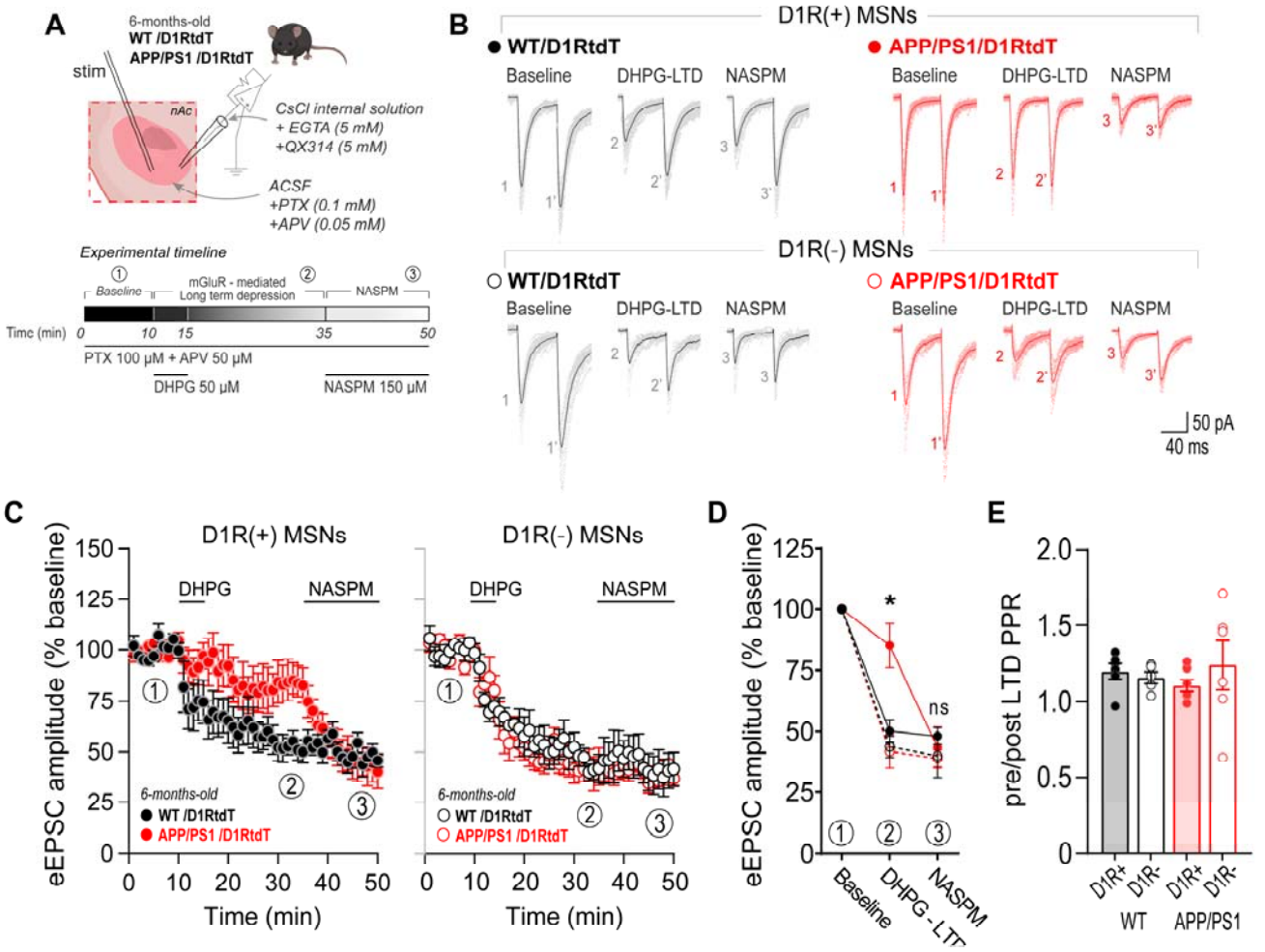

Fig. 6 | Impaired mGluR1/5-dependent LTD and CP-AMPAR dysregulation in D1R+ medium spiny neurons of the nucleus accumbens in APP/PS1 mice. A Schematic of whole-cell voltage-clamp recordings performed in MSNs from the nAc of 6-month-old WT/D1RtdT and APP/PS1/D1RtdT mice. D1R+ MSNs were identified by tdTomato expression. After baseline acquisition, LTD was induced by bath application of DHPG (50 µM, 5 min), followed by application of NASPM (150 µM). **B** Representative AMPAR-mediated eEPSC traces recorded from D1R+ and D1R− MSNs at baseline, after DHPG-induced LTD, and during NASPM application in WT and APP/PS1 mice. Overlaid traces show individual responses (light) and averages (dark). Paired-pulse responses were obtained using double-pulse stimulation (Δt = 70 ms). **C** Time course of

normalized eEPSC amplitudes (% baseline) in D1R+ (left) and D1R− (right) MSNs. DHPG-induced LTD was markedly reduced in D1R+ MSNs from APP/PS1 mice and partially restored by NASPM, whereas D1R− MSNs exhibited comparable LTD between genotypes. Black bars indicate periods of DHPG and NASPM application. **D** Quantification of normalized eEPSC amplitudes at baseline, after DHPG-LTD, and during NASPM application. A mixed-effects REML analysis revealed significant main effects of stage ($F(1.845, 36.90) = 127.7$, $p < 0.001$), genotype ($F(3, 20) = 4.292$, $p = 0.017$), and a stage × genotype interaction ($F(6, 40) = 5.105$, $p < 0.001$). Tukey's post hoc tests showed reduced LTD in APP/PS1 D1R+ MSNs compared with WT D1R+ ($p = 0.039$) and APP/PS1 D1R− MSNs ($p = 0.014$). **E** Quantification of paired-pulse ratio (PPR; post/pre LTD) revealed no significant differences among groups (Kruskal–Wallis test, $H(3) = 1.928$, $p = 0.587$; Dunn's multiple comparisons test, all adjusted $p > 0.999$). Data are presented as mean ± s.e.m. Each data point represents a single recorded neuron.

Dopaminergic hypoactivity and reward-related behavioral alterations in the nAc of APP/PS1 mice at pre-plaque stage.

To determine whether the early synaptic alterations identified in the nAc of APP/PS1 mice are accompanied by changes in local dopaminergic signaling, dopamine dynamics were assessed using the genetically encoded fluorescent sensor dLight1.1, which was stereotaxically injected into the nAc (Fig. 7A). Acute slice photometry revealed that electrical stimulation evoked robust dopamine-dependent fluorescence transients in nAc-containing slices from WT mice, whereas slices from APP/PS1 mice displayed markedly reduced responses (Fig. 7B). Consistently, input–output curves demonstrated

462 a significant reduction in normalized dLight1.1 fluorescence across stimulus intensities
463 in APP/PS1 mice compared with WT controls (Fig. 7C), indicating impaired evoked
464 dopaminergic signaling in the nAc at pre-plaque stages.

465 We next investigated whether this dopaminergic hypoactivity was associated with
466 alterations in reward-related behavior. Using a conditioned place preference (CPP)
467 paradigm using chocolate (Fig. 7D), mice first underwent a pre-conditioning session to
468 assess baseline context preference. APP/PS1 mice exhibited a significant bias toward
469 the small-grid context during this phase, whereas WT mice showed no preference (Fig.
470 7E), indicating altered exploratory behavior in the absence of reward. During
471 conditioning, the chocolate-paired context (Cs+) was counterbalanced based on
472 individual baseline preference. In the CPP test, both WT and APP/PS1 mice spent
473 significantly more time in the reward-associated context compared with the non-
474 rewarded context (Fig. 7F), demonstrating intact associative learning in both genotypes,
475 albeit with a stronger CPP expression in APP/PS1 mice.

476 Despite comparable CPP learning, APP/PS1 mice consumed significantly more
477 chocolate across conditioning days than WT mice (Fig. 7G), whereas pellet
478 consumption did not differ between genotypes (Fig. 7H). This selective increase in
479 palatable reward intake suggests altered reward valuation in APP/PS1 mice rather than
480 generalized changes in feeding behavior.

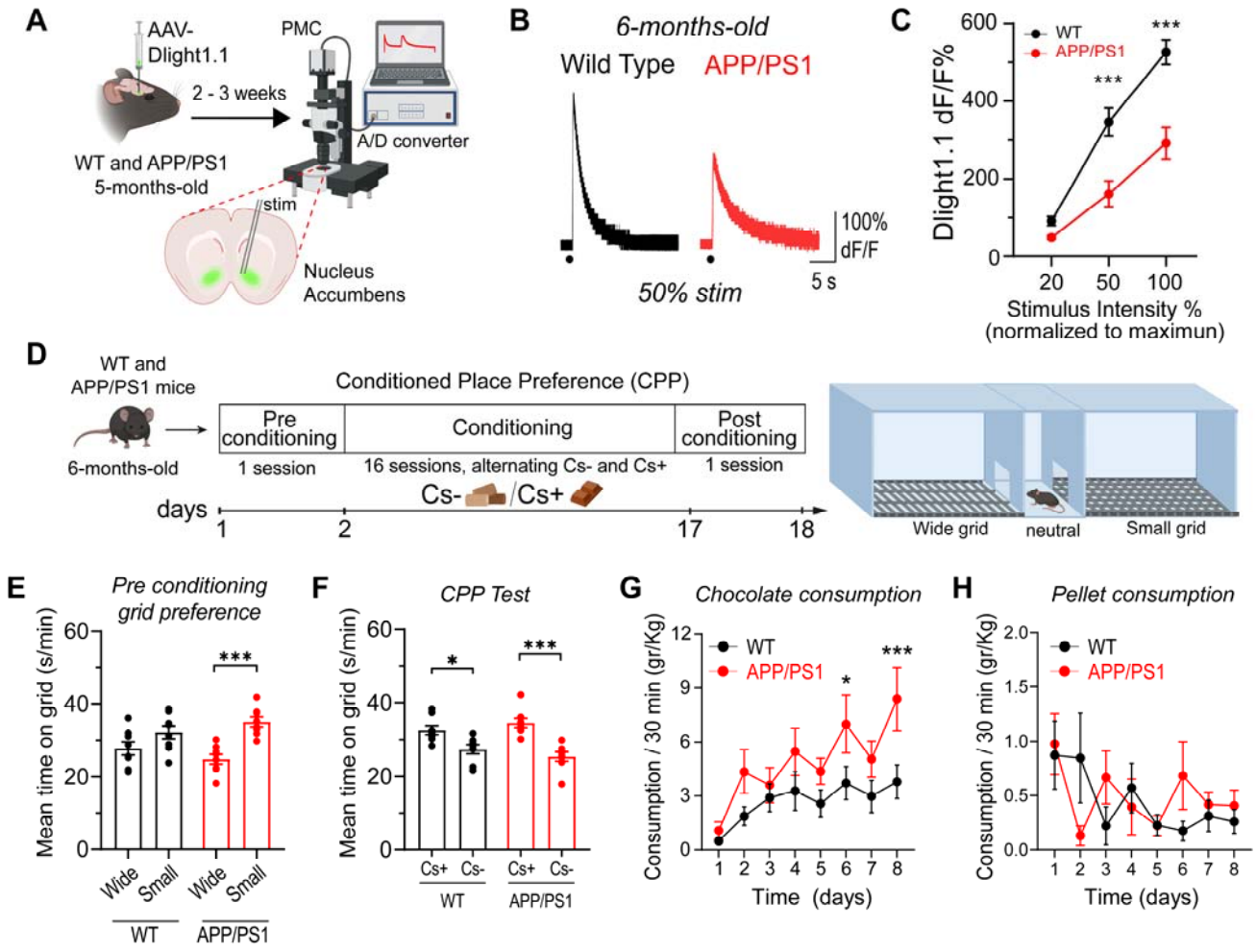

Fig. 7 | Reduced dopamine-dependent signaling in the nucleus accumbens and altered reward-related behavior in APP/PS1 mice. A AAV-dLight1.1 was injected into the nAc of WT and APP/PS1 mice and allowed to express for 2–3 weeks before acute slice preparation for dopamine imaging. Dopamine-dependent fluorescence signals were recorded using slice photometry following electrical stimulation. **B** Representative dLight1.1 fluorescence traces evoked by electrical stimulation in nAc slices from 6-month-old WT (black) and APP/PS1 (red) mice. **C** Input–output relationship between normalized dLight1.1 fluorescence (ΔF/F%) and stimulus intensity reveals a reduced dopamine-dependent signal in APP/PS1 mice (WT: n = 12 slices from 4 mice;

APP/PS1: n = 10 slices from 3 mice; two-way ANOVA with Bonferroni post hoc test, ***p < 0.001). **D** Schematic of the conditioned place preference (CPP) experimental design, including pre-conditioning, conditioning, and post-conditioning phases, using wide and small grid contexts. **E** Pre-conditioning analysis of grid preference shows increased baseline preference for the small grid in APP/PS1 mice compared with WT (two-way ANOVA, grid type effect $F(1,14) = 22.04$, $P < 0.001$; WT, $P = 0.121$; APP/PS1, $P < 0.001$). **F** CPP test reveals increased time spent in the reward-associated context (Cs+) compared with the non-rewarded context (Cs−) in both genotypes, with a stronger effect in APP/PS1 mice (two-way ANOVA, interaction $F(1,14) = 6.25$, $P = 0.0254$; grid effect $F(1,14) = 21.90$, $P = 0.0004$; genotype effect $F(1,14) = 3.047 \times 10E3$, $P > 0.999$; Bonferroni post hoc test, WT $P = 0.012$, APP/PS1 $P < 0.0001$). **G** Chocolate consumption during the conditioning phase is increased in APP/PS1 mice compared with WT across days (two-way ANOVA, time effect $P < 0.0001$; Bonferroni post hoc test, day 6 $P = 0.0171$, day 8 $P = 0.0003$). **H** Pellet consumption during conditioning shows no significant differences between genotypes. Data are presented as mean ± s.e.m. unless otherwise indicated. n = 8 mice per genotype.

To determine whether the alterations in reward-related behavior observed in APP/PS1 mice extended to other affective or social domains, anxiety-like behavior and sociability were evaluated using the elevated plus maze and a three-chamber social interaction paradigm, respectively (Fig. 5S). In the elevated plus maze, WT and APP/PS1 mice exhibited comparable time spent in the open and closed arms, similar numbers of arm entries, and equivalent distances traveled, indicating no genotype-dependent differences in anxiety-like behavior (Fig. 5S, A-G). Likewise, in the social interaction

task, both genotypes showed intact social preference and social novelty, as evidenced by comparable time spent in each chamber and similar sniffing times toward conspecific versus empty or novel stimuli (Fig. 5S, I-M).

Together, these results indicate that anxiety-like responses and social behaviors remain preserved in APP/PS1 mice at this stage, suggesting that the behavioral phenotype associated with dopaminergic hypoactivity in the nucleus accumbens is selective for reward-related processes. Notably, these circuit-level and behavioral alterations emerge at pre-plaque stages, supporting the idea that accumbal dysfunction precedes extracellular Aβ deposition.

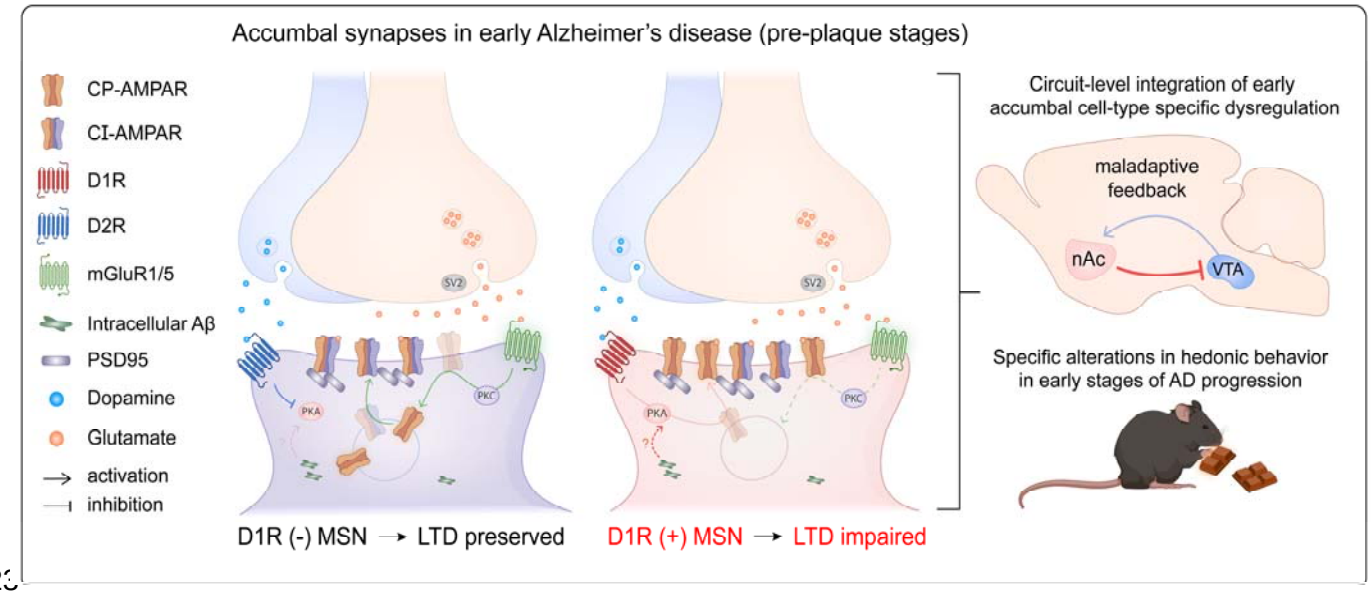

Fig. 8 | Proposed mechanistic model underlying selective synaptic plasticity impairment in the nucleus accumbens during early stages of Alzheimer's disease. Schematic model illustrating the integration of glutamatergic and dopaminergic signaling onto nAc MSNs during pre-plaque stages of AD, when intracellular Aβ is present in the absence of extracellular plaques. Both synapses depicted correspond to the AD

condition. In D1R-negative MSNs (left, purple; putatively D2R-expressing), synaptic plasticity is preserved despite intracellular Aβ accumulation, consistent with intact mGluR1/5 signaling and putatively reduced engagement of PKA-dependent pathways. In contrast, D1R-expressing MSNs (right) exhibit impaired mGluR1/5-dependent LTD, leading to deficient AMPAR endocytosis and persistent functional presence of CP-AMPARs. Reduced dopaminergic tone may preferentially weaken D1R-dependent signaling, allowing intracellular Aβ to promote PKA-dependent AMPAR stabilization, potentially facilitated by increased PSD-95. At the circuit level, these early, cell-type-specific alterations are proposed to bias mesolimbic output and contribute to selective changes in reward-related behavior during early AD.

DISCUSSION

The present study shows that excitatory neurotransmission and synaptic plasticity in the nucleus accumbens were disrupted at 6 months in a cell type–specific manner, preferentially affecting D1R-expressing medium spiny neurons during pre-plaque stages in APP/PS1 mice. The phenotype included impaired LTD, enhanced calcium-permeable AMPAR, reduced dopamine signaling, and a selective alteration in a reward-related behavior. Together, these results identify the accumbens direct pathway as an early site of synaptic vulnerability before plaque deposition and cognitive decline in the APP/PS1 model (see Fig. 8).

AD is increasingly recognized as a brain disorder that perturbs distributed neural circuits well before memory impairment becomes clinically evident [24, 47]. Although research has traditionally focused on hippocampal and cortical regions, important for learning and

551 memory, converging evidence shows that non-cognitive symptoms, including apathy,
552 motivational deficits, and affective disturbances, often precede cognitive decline [4, 48, 49].
553 These early neuropsychiatric manifestations implicate limbic and reward-related circuits,
554 whose underlying molecular and synaptic mechanisms remain poorly understood [6, 46].

555 The nAc is a central integrative hub of the mesolimbic system that modulates affective
556 processing, motivation, and reward-related behaviors [18, 23], positioning it as a key
557 contributor to early disease phenotypes. In humans, nAc atrophy has been reported in
558 patients with AD and correlates with cognitive performance, while increased
559 inflammation is associated with reduced functional connectivity between the nAc and
560 cortical regions involved in decision-making and inhibitory control [19, 20]. Despite this
561 observation, the nAc has remained relatively underexplored in experimental models of
562 Alzheimer's disease. By focusing on the nAc during pre-plaque stages, the present
563 study addresses this gap and supports the notion that early AD pathology cannot be
564 fully explained by hippocampal and cortical dysfunction alone.

565 A critical aspect in interpreting Alzheimer's disease mechanisms is the temporal
566 framework in which the pathology is examined [6, 50]. While most studies have focused on
567 advanced stages characterized by extracellular amyloid plaques and established
568 cognitive deficits [8, 9, 51, 52], converging evidence from human tissue and animal models
569 indicates that intracellular amyloid-beta accumulation, increased excitatory
570 transmission, and neuropsychiatric symptoms precede plaque formation [7, 12, 53, 54].
571 Consistent with this view, transgenic models differ markedly in their temporal
572 trajectories, supporting the existence of an early disease phase in which initial cellular

and synaptic alterations occur before classical neuropathological hallmarks emerge [55-57].

A central finding of this study is the progressive and cell-type specific disruption of long-term depression in the nucleus accumbens during early AD stages. LTD was preserved at 3 months of age, but markedly impaired at 6 months, indicating a gradual loss of synaptic plasticity as the pathology advances. Importantly, although intracellular Aβ accumulation was comparable in D1R-positive and D1R-negative MSNs, LTD impairment was selectively observed in D1R-expressing neurons. This dissociation indicates that intracellular Aβ accumulation is necessary but not sufficient to disrupt synaptic plasticity. Rather, our data show that intrinsic properties linked to MSN subtype identity confer selective vulnerability to intracellular Aβ effects.

The selective alteration of D1R-positive neurons in AD aligns with observations from addiction and withdrawal paradigms, in which synaptic plasticity and AMPAR remodeling are preferentially disrupted in D1R-expressing MSNs of the nAc [36, 58]. These parallels suggest that convergent mechanisms of synaptic vulnerability may operate across distinct pathological contexts. Consistent with this view, dietary restriction in mice reduces dopamine release in the nAc, triggering a compensatory increase in D1R-dependent signaling that promotes AMPAR remodeling and leads to more persistent reward-seeking behavior than under unrestricted feeding conditions [40].

Our data demonstrate aberrant AMPAR subunit remodeling as a key mechanism underlying the loss of LTD in D1R-expressing MSNs. Increased inward rectification, enhanced sensitivity to NASPM, a decreased +40 mV AMPAR/NMDAR ratio, and

595 increased calcium-permeable AMPAR component revealed by GCaMP-based calcium
596 imaging collectively support the functional incorporation of GluA2-lacking, calcium-
597 permeable AMPARs at accumbal synapses in APP/PS1 mice. Notably, although both
598 HFS-LTD and mGluR1/5-LTD were broadly impaired in 6-month-old APP/PS1 mice, cell-
599 type–specific analyses in APP/PS1/D1RtdTomato animals allowed us to identify D1R-
600 expressing MSNs as the principal cell-type contributing to these synaptic deficits.

601 The alteration of CP-AMPARs in D1R-expressing MSNs during pre-plaque stages may
602 arise from convergent disruptions in glutamatergic and dopaminergic signaling. One
603 possibility is the impairment of mGluR1/5-dependent plasticity. In the nAc, mGluR1/5-
604 mediated LTD normally constrains synaptic strength by promoting AMPAR endocytosis
605 and subunit exchange, favoring the removal of GluA2-lacking CP-AMPARs and the
606 insertion of GluA2-containing AMPARs of lower conductance [28]. The persistent synaptic
607 presence of CP-AMPARs indicates impaired mGluR1/5-dependent plasticity, as
608 pharmacological blockade of CP-AMPARs selectively restored mGluR1/5-LTD in D1R-
609 positive MSNs.

610 This mGluR1/5-LTD–CP-AMPAR mechanism is consistent with dysfunctional plasticity
611 observed in other pathological contexts. In addictive models, CP-AMPAR accumulation
612 in the nAc arises from loss of mGluR1/5-dependent LTD driving persistent reward-
613 seeking behavior [36, 59]. Using extracellular field recordings at CA3–CA1 synapses,
614 Valdivia et al. reported an age-dependent decline in hippocampal mGluR-dependent
615 LTD in APP/PS1 mice, which was preserved at 2 months but reduced by 8 months [60].
616 The present study combines intracellular recordings with genetic cell-type identification
617 to demonstrate that mGluR-LTD impairment emerges earlier in a distinct mesolimbic

618 region and is selectively expressed in D1R-expressing MSNs, where it is directly
619 associated with aberrant CP-AMPAR accumulation. Together, these observations
620 highlight how differences in circuit, disease stage, and experimental resolution critically
621 shape the manifestation of mGluR-dependent synaptic dysfunction in AD.

622 The selective vulnerability of D1R-expressing MSNs likely reflects their dependence on
623 dopaminergic tone. D1 receptors exhibit lower affinity for dopamine than D2 receptors,
624 rendering D1R-positive neurons particularly sensitive to reductions in dopamine
625 availability [61, 62]. Consistent with this notion, we found a reduced dopamine-dependent
626 signaling in the nAc at 6 months of age using a genetically encoded sensor. These
627 findings align with previous reports showing that dopamine release in the nAc is
628 significantly reduced during pre-plaque stages in the APPswe mice, accompanied by a
629 compensatory decrease in dopamine transporter expression [45]. Although our results do
630 not distinguish between impaired presynaptic release, dopaminergic terminal
631 dysfunction, or early degeneration of VTA neurons, any reduction in dopamine
632 availability would be expected to disproportionately weaken D1R-mediated signaling.
633 Such dopaminergic hypoactivity may therefore converge with Aβ-driven postsynaptic
634 alterations to destabilize direct pathway function during early stages of AD. For
635 instance, Whitcomb et al. reported that intracellular perfusion of Aβ oligomers into
636 hippocampal neurons rapidly increase surface GluA1 and promote CP-AMPAR insertion
637 through a PKA-dependent pathway [42]. Thus, a reduced dopaminergic tone may weaken
638 physiological D1R-PKA coupling, developing conditions in which intracellular Aβ
639 aberrantly engages PKA signaling to drive GluA1 membrane insertion. In contrast, D2R
640 signaling inhibits adenylyl cyclase and suppresses PKA activity [63], potentially limiting

this mechanism in D2R+ MSNs and contributing to their marked resilience. Together, impaired mGluR1/5-dependent AMPAR endocytosis and Aβ-driven GluA1 insertion would bias synapses toward persistent CP-AMPAR enrichment, providing a mechanistic explanation for the selective failure of LTD in D1R+ MSNs during early Alzheimer's disease.

In agreement with the present results, Aguado et al. reported that CP-AMPAR are increased in the hippocampus of APPswe mice at advanced stages of the disease, particularly in animals displaying a vulnerable phenotype [64]. Notably, mGluR5 expression was reduced in vulnerable APPswe animals, but preserved in resilient mice, paralleling the normalization of CP-AMPAR expression [64]. These findings suggest that coordinated regulation of mGluR1/5 signaling and CP-AMPAR composition may act as a compensatory mechanism modulating synaptic vulnerability across disease stages and brain regions. Complementing this view, Guo et al. demonstrated that acute exposure to exogenous oligomeric Aβ in the nAc of young WT mice induces synaptic insertion of CP-AMPARs, leading to spine loss, synaptic weakening, and motivational deficits [65]. Importantly, this model reflects extracellular Aβ-driven pathology and preferentially impacts D2 MSNs, contrasting with our findings showing that intracellular Aβ accumulation during early stages selectively promotes CP-AMPAR incorporation in D1R-expressing MSNs. Together, these studies highlight CP-AMPAR dysregulation as a convergent mechanism of synaptic failure across disease stages.

The nucleus accumbens functions as a critical inhibitory hub within the mesolimbic circuit, regulating reward-related signal gain through the integration of glutamatergic inputs and dopaminergic modulation [17]. The selective loss of LTD in D1R-expressing

MSNs is therefore expected to bias circuit output toward enhanced direct pathway activity, reducing the capacity of the nAc to constrain excitatory drive and favoring reward-seeking behavior. In parallel, reduced dopaminergic tone may further weaken D1R signaling, potentially causing compensatory increases in reward consumption to achieve comparable motivational salience. Our data reveal selective changes in reward valuation, including increased consumption of palatable solid food and altered preference behavior, in the absence of anxiety-like or social deficits. Together, these findings suggest that early synaptic dysfunction within the nAc preferentially disrupts motivational processing rather than broader affective domains.

Some limitations should be considered when interpreting these findings. First, all experiments were performed in male mice, precluding assessment of sex-specific mechanisms. This is particularly relevant given evidence that estradiol signaling profoundly modulates synaptic plasticity within the nucleus accumbens. Estradiol, acting through mGluR5 and endocannabinoid signaling, has been shown to structurally remodel nAc reward circuits and enhance sensitivity to psychostimulants [66], highlighting a strong interaction between hormonal state and mesolimbic plasticity. Second, although our data reveal a robust association between intracellular Aβ accumulation and synaptic alterations, the APP/PS1 model does not allow definitive attribution of these effects exclusively to Aβ. Nonetheless, prior studies support a direct role for intracellular Aβ in modulating excitatory synaptic function. Fernández-Pérez et al. demonstrated that intracellular Aβ enhances neuronal synchronization and AMPAR-mediated transmission [67], and Saavedra et al. reported increased intracellular Aβ levels together with augmented AMPAR currents in cultured nAc MSNs derived from APP/PS1 mice [68].

Together, these observations support a direct contribution of intracellular Aβ to the synaptic alterations described here, while underscoring the need for future studies incorporating sex as a biological variable and approaches that selectively manipulate intracellular Aβ levels to establish causality.

In conclusion, this study identifies early synaptic alterations in which intracellular Aβ accumulation is associated with disrupted AMPAR subunit composition, selective impairment of LTD in D1R-expressing MSNs, reduced dopaminergic signaling in the nAc before extracellular Aβ plaque deposition, and specific hedonic behavior alterations. These findings suggest that non-cognitive symptoms in Alzheimer's disease may reflect early circuit-level imbalance rather than late-stage neurodegeneration. By highlighting the nucleus accumbens as an early site of vulnerability, this work underscores the importance of neuronal subtype identity and signaling context in shaping susceptibility to the early intracellular Aβ accumulation.

METHODS

Animals

All experimental procedures were approved by the Institutional Animal Care and Use Committee of the University of Concepción and were conducted in accordance with national and international guidelines for the care and use of laboratory animals. Male C57BL/6J mice, double-transgenic APPswe/PS1dE9 mice (MMRRC:034832; B6.Cg-Tg(APPswe,PSEN1dE9)85Dbo/Mmjax), and Drd1a-tdTomato reporter mice (B6.Cg-Tg(Drd1a-tdTomato)6Calak/J; JAX stock #016204) were obtained from The Jackson Laboratory (Bar Harbor, ME, USA) and maintained at the Regional Center for Advanced

Studies in Life Sciences (CREAV), University of Concepción. The transgenic line expresses the Swedish mutation (K594M/N595L) in amyloid precursor protein (APP) and the human presenilin-1 variant lacking exon 9 (PS1-dE9), leading to an increased Aβ production [69]. Drd1a-tdTomato mice express the fluorescent reporter tdTomato under the control of the dopamine D1 receptor (Drd1a) promoter, allowing selective visualization of D1R-expressing medium spiny neurons [70]. To generate experimental cohorts enabling recordings from genetically labeled D1R-expressing MSNs, D1RtdTomato mice were crossed with APP/PS1 mice to obtain APP/PS1/D1RtdTomato offspring; WT/D1RtdTomato littermates were used as controls for these experiments. Genotyping was performed according to the provider's instructions for each line. Mice were housed in groups of 2–5 under a 12 h light/dark cycle with ad libitum access to food and water. Animals were used between 3 and 12 months of age. Euthanasia was performed by decapitation following anesthesia with inhaled isoflurane.

Immunohistochemistry

Mice were anesthetized with ketamine (100 mg/kg, i.p.) and xylazine (10 mg/kg, i.p.) and transcardially perfused with pre-warmed saline (0.9% NaCl, 35 °C), followed by freshly prepared ice-cold 4% paraformaldehyde (PFA). Brains were then dissected, post-fixed for 24 h at 4 °C, and cryoprotected in 30% sucrose for 3–5 days at 4 °C. Samples were embedded in NEG50, cooled at −20°C for 2-4 h, and stored at −80°C for at least 24 h before sectioning with a cryostat. Free-floating coronal sections (30 µm) were rinsed in Tris-phosphate buffer, permeabilized in Trisphosphate containing 1% BSA and 0.2% Triton X-100, and incubated for 24 h at 4°C with primary antibodies: MOAβ-2 (1:200, mouse, Novus Biologicals, USA), MAP2 (1:200, guinea pig, Synaptic

Systems, Germany), and Iba1 (1:1000, rabbit, Alomone Labs, Germany). Sections were then incubated for 2 h with secondary antibodies (Alexa Fluor 488, Alexa Fluor 594, Alexa Fluor 647). Stained samples were mounted with DAKO fluorescent medium on glass slides and imaged using confocal microscopy at the Advanced Microscopy Center (CMA, Biobío). For each animal, at least two coronal sections were analyzed, with three distinct regions of interest (ROIs) per section. Each ROI was consistently acquired as a Z-stack (~20 µm) for subsequent processing and quantification using FIJI and Zen software.

Thioflavin-S staining

Thioflavin-S (Sigma, T1892), which binds β-sheet–rich structures present in amyloid aggregates, was used to assess extracellular amyloid plaque deposition. Coronal brain sections (35 µm) containing the nucleus accumbens and hippocampus were mounted on glass slides and processed at room temperature (~22 °C). Sections were dehydrated through a graded ethanol series (50%, 70%, 80%, 90%, 95%, and 100%; 5 min each), incubated in xylene (Winkler, XI-1670) for 10 min, and subsequently rehydrated through descending ethanol concentrations (100%, 95%, 90%, 80%, and 70%; 5 min each). Freshly prepared Thioflavin-S solution (0.05% in 50% ethanol) was filtered prior to use, and sections were incubated for 10 min protected from light. Sections were then washed in 70% ethanol (3 min) followed by distilled water (2 min), coverslipped, and stored protected from light until imaging. Images were acquired using confocal microscopy with identical acquisition parameters across genotypes and brain regions. For each animal, five sections were analyzed, sampled every 100 µm, and four animals per group were included. Autofluorescence background was estimated from negative

control sections processed without Thioflavin-S and subtracted from all images. Fluorescent puncta larger than 5 µm were considered amyloid plaques. Absence of detectable Thioflavin-S signal was interpreted as absence of plaque deposition. The analysis was performed blinded to genotype. Quantification was conducted within the same regions of interest used for immunohistochemical analyses.

Electrophysiological recordings in coronal brain slices

Acute coronal brain slices containing the nucleus accumbens were prepared from male mice anesthetized with isoflurane and euthanized by decapitation. Brains were rapidly removed and transferred to an ice-cold, oxygenated cutting solution containing (in mM): 194 sucrose, 30 NaCl, 4.5 KCl, 1.2 $NaH_2PO_4 \cdot H_2O$, 1 $MgCl_2 \cdot 6H_2O$, 26 $NaHCO_3$, and 10 glucose (pH 7.4, equilibrated with 95% O_2/5% CO_2). Coronal slices (300 µm) were prepared using a vibratome (VT1200, Leica, Germany) and allowed to recover for 1 h at 32°C in artificial cerebrospinal fluid (aCSF) containing (in mM): 124 NaCl, 26 $NaHCO_3$, 10 glucose, 4.5 KCl, 2 $CaCl_2 \cdot 2H_2O$, 1 $MgCl_2 \cdot 6H_2O$, and 1.2 $NaH_2PO_4 \cdot H_2O$, continuously bubbled with 95% O_2/5% CO_2.

Whole-cell patch-clamp recordings were performed in the nucleus accumbens core using an Axopatch 200B amplifier coupled to a Digidata 1440A digitizer and pClamp 10 software (Axon Instruments). Recording pipettes (4–5 MΩ) were pulled from borosilicate glass capillaries (WPI) using a horizontal puller (P-1000, Sutter Instruments). During recordings, slices were continuously perfused with oxygenated aCSF at 32°C. Signals were low-pass filtered at 2 kHz and digitized at 10 kHz. Series resistance was continuously monitored and partially compensated (60–70%) throughout the recordings; cells were excluded if series resistance changed by more than 20%.

Voltage Clamp recordings

For voltage-clamp experiments, the internal pipette solution contained (in mM): 120 CsCl, 10 HEPES, 4 MgCl2·6H2O, 2 Mg-ATP, 0.5 Na2-GTP, and 10 BAPTA (tetra-Cs) (pH 7.4, adjusted with CsOH; 290 mOsm), together with QX-314 (1 mM) and TEA-Cl (5 mM). For rectification index experiments, Spermine (100 µM) was also included. For DHPG-induced LTD experiments, EGTA (1 mM) was used instead of BAPTA. Bath solutions were continuously perfused at a rate of 1 mL/min.

Spontaneous synaptic currents.

Spontaneous excitatory postsynaptic currents (sEPSCs) were recorded at a holding potential of −60 mV. AMPAR-mediated events were isolated by bath application of picrotoxin (PTX, 100 µM) to block GABAA and glycine receptors, and D-AP5 (50 µM) to block NMDA receptors. After break-in, cells were allowed to stabilize for at least 10 min before recording. sEPSCs were recorded under baseline conditions and subsequently in the presence of PTX and D-AP5 for a minimum of 15 min. Event detection was performed using the template search algorithm in Clampfit v11, and at least 300 events per cell were analyzed. Parameters quantified included event frequency, amplitude, rise time, and decay time.

Synaptic stimulation and evoked responses.

Evoked excitatory postsynaptic currents (eEPSCs) were elicited using a tungsten bipolar stimulating electrode (World Precision Instruments) positioned approximately 100 µm from the recorded neuron and connected to an isolated pulse stimulator (A-M Systems). Square current pulses (1 ms, 0.05–0.5 mA) were delivered to evoke stable

responses with amplitudes ≤200 pA. Stimulation intensity was adjusted only at the beginning of each recording to obtain a stable response and was not modified thereafter. Baseline recordings were initiated only after achieving stable eEPSCs that varied by no more than 30% over a period exceeding 1 min (corresponding to at least three consecutive sweeps, delivered every 20 s).

AMPA/NMDA ratio.

AMPAR- and NMDAR-mediated components were measured from eEPSCs recorded in the presence of PTX (100 µM). AMPAR responses were obtained at −60 mV. The holding potential was then shifted to +40 mV to record mixed AMPA+NMDA responses (30 sweeps, one every 20 s). D-AP5 (50 µM) was subsequently applied to isolate the AMPAR component at +40 mV. The NMDA component was calculated by subtracting the averaged AMPAR trace from the mixed response, and its amplitude was measured 20 ms after the peak of the AMPAR current. The AMPA/NMDA ratio was calculated as the peak AMPAR current divided by the NMDA current amplitude.

Paired-pulse ratio (PPR).

Paired-pulse ratio (PPR) was assessed at −60 mV using two consecutive stimuli delivered with a 70 ms inter-stimulus interval. PPR was calculated as the ratio between the second and first eEPSC amplitudes (R2/R1), using responses ≤200 pA.

Rectification index (RI).

Rectification properties of AMPAR-mediated currents were assessed using CsCl-based internal solution containing spermine (100 µM), in the presence of PTX (100 µM) and D-AP5 (50 µM). eEPSCs were recorded at holding potentials ranging from −60 to +40 mV

in 20 mV increments. For each potential, 30 sweeps were collected and averaged. The rectification index was calculated as the ratio of the absolute current amplitude at +40 mV to that at −60 mV.

NASPM sensitivity.

To assess the contribution of calcium-permeable AMPARs, MSNs were voltage-clamped at −60 mV. After establishing a stable baseline for at least 10 min (one stimulus every 20 s), NASPM (150 µM) was bath-applied for a minimum of 15 min. Inhibition was expressed as the percentage reduction in mean eEPSC amplitude, comparing baseline responses with those recorded during the last 5 min of NASPM application.

Long-term depression (LTD)

All LTD experiments were performed in the presence of PTX (100 µM) and D-AP5 (50 µM). For HFS-induced LTD, recordings were obtained with CsCl-based internal solution. After recording a stable baseline for at least 10 min, LTD was induced using four trains of stimuli delivered at 100 Hz (1 ms pulses), separated by 20 s. eEPSCs were recorded for at least 40 min following induction. LTD magnitude was calculated as the percentage change in normalized eEPSC amplitude during the last 5 min relative to baseline.

For mGluR1/5-dependent LTD, recordings were performed using internal solution containing EGTA (1 mM). After a stable 10 min baseline, (RS)-3,5-dihydroxyphenylglycine (DHPG, 50 µM) was bath-applied for 5 min, and eEPSCs were monitored for at least 25 min thereafter. LTD magnitude was calculated as the

843 percentage reduction in mean eEPSC amplitude during the final 5 min relative to
844 baseline.

845 **Experimental design and analysis**

846 The number of cells and animals analyzed for each experiment is reported in the
847 corresponding figure legends. Animals were randomly selected for recordings without
848 prior knowledge of their APP/PS1 or WT genotype; only tdTomato fluorescence was
849 used to identify D1R-expressing neurons when applicable. Data acquisition and
850 analysis were performed blind to genotype.

851 **Stereotaxic injections**

852 Five-month-old male WT and APP/PS1 mice were used. Stereotaxic surgery was
853 performed to deliver adeno-associated viruses (AAVs) expressing the genetically
854 encoded calcium indicator GCaMP6s under the synapsin promoter, as previously
855 described [22]. A total of 200 nL of AAV1-Syn-GCaMP6s.WPRE.SV40 (1.76×10^{13} GC/ml;
856 Addgene #100843-AAV1) or or 400 nL of pAAV-CAG-dLight1.1 (7×10^{12} vg/ml;
857 Addgene #111067-AAV5) was injected bilaterally into the nucleus accumbens (nAc)
858 using a stereotaxic alignment system (Kopf Instruments). Injection coordinates relative
859 to bregma were: AP +0.13 mm, ML ±0.11 mm, and DV −0.4 mm (Allen Brain Atlas).
860 Mice were anesthetized with 4% isoflurane/oxygen and positioned in a stereotaxic
861 frame; anesthesia was maintained with 2–3% isoflurane/oxygen throughout the
862 procedure. After leveling the skull, a small craniotomy was made at the target site. A 1
863 µL Neuros Hamilton syringe was lowered slowly to the desired depth, and viral solution

was delivered. The syringe was left in place for 1 min post-infusion before withdrawal, and incisions were closed with Leukosan adhesive.

Calcium and Dopamine photometry

Two to three weeks after AAV injection, mice are 6 months old and completely recovered. Acute coronal slices (300 µm) containing the nAc were prepared for calcium or dopamine imaging. Slices were transferred to an upright microscope and continuously perfused with oxygenated aCSF (1 mL/min). The recording region of interest (medial to the anterior commissure, corresponding to the nAc core) was visualized under fluorescence to confirm GCaMP6s or Dlight1.1 expression. A bipolar stimulating electrode (DS3 Isolated Current Stimulator, Digitimer, UK) was placed on the slice surface near the area of interest. Stimulation consisted of single electrical pulses (400–800 µA, 1 ms duration, 10 Hz). Transients were measured by slice photometry using a Horiba PTI D-104 Microscope Photometer with a 710 nm photomultiplier tube mounted on an Olympus BX51 microscope, equipped with a 120 LED Boost High-Power illumination system and appropriate fluorescence filters. Fluorescence signals were acquired using Patch-Master software and expressed as $\Delta F/F_0$. Single-pulse electrical stimulation was delivered every 2 min, generating one evoked fluorescence transient per stimulus. A stable baseline was recorded for 12 min (six responses), followed by bath application of the AMPAR antagonist CNQX and continued stimulation for an additional 12 min until responses reached a plateau. For analysis, $\Delta F/F_0$ values were normalized to baseline and expressed as percentage change. Drug effects were quantified by comparing the mean response during the last 6 min in the presence of CNQX with baseline for each slice. Data represent individual

887 slices obtained from at least three animals per experimental group, and analyses were
888 performed blind to genotype.

889 **Western blot**

890 The nAc was microdissected from coronal slices of 6-months-old WT and APP/PS1
891 male mice. Tissue was homogenized in RIPA buffer containing protease and
892 phosphatase inhibitors, and protein concentration was determined by BCA assay. Equal
893 amounts of protein (50 µg) were separated by SDS–PAGE and transferred to PVDF
894 membranes. Membranes were blocked in 5% non-fat milk and incubated overnight at 4
895 °C with primary antibodies against SV2, PSD95, GluA1, GluA2, and Gβ (loading
896 control). After incubation with HRP-conjugated secondary antibodies, proteins were
897 visualized by ECL and imaged on a chemiluminescence detection system. Band
898 intensities were quantified in FIJI, normalized to Gβ, and expressed relative to WT
899 controls.

900 **qRT-PCR**

901 The nAc was microdissected from 300 µm coronal brain slices. Total RNA was
902 extracted using TRIzol reagent according to the manufacturer's instructions and treated
903 with DNase to eliminate potential genomic DNA contamination. Complementary DNA
904 (cDNA) was synthesized from 2 µg of total RNA using reverse transcriptase and
905 oligo(dT) primers. Quantitative real-time PCR was performed for 40 cycles using SYBR
906 Green Universal Master Mix (Agilent Technologies) and gene-specific primers targeting
907 NMDA receptor subunits and AMPA receptor subunits. The following primer pairs were
908 used: Gria1 (GluA1), forward 5′-ACCCTCCATGTGATCGAAATG-3′ and reverse 5′-

GGTTCTATTCTGGACGCTTGAG-3′; Gria2 (GluA2), forward 5′-AAAGAATACCCTGGAGCACAC-3′ and reverse 5′-CCAAACAATCTCCTGCATTTCC-3′; Grin1 (NMDA receptor subunit 1), forward 5′-AAATGTGTCCCTGTCCATACTC-3′ and reverse 5′-CCTGCCATGTTCTCAAAAGTG-3′; Grin2b (NMDA receptor subunit 2B), forward 5′-GAACGAGACTGACCCAAAGAG-3′ and reverse 5′-CAGAAGCTTGCTGTTCAATGG-3′. Cyclophilin A was used as the housekeeping gene, with forward primer 5′-ATAATGGCACTGGTGGCAAGTC-3′ and reverse primer 5′-ATTCCTGGACCCAAAACGCTCC-3′. Relative mRNA expression levels were calculated using the ΔΔCt method and expressed as fold changes relative to WT controls..

Statistical analysis

All electrophysiological data were analyzed using Clampfit v11 (Molecular Devices). Synaptic event detection was performed using the template search protocol implemented in Clampfit. Data were organized in Microsoft Excel and subsequently imported into GraphPad Prism (version 10) for statistical analyses and figure preparation. Normality was assessed using the Shapiro–Wilk test. For comparisons between two independent groups, unpaired two-tailed Student's t-tests or Welch's t-tests were used when variance was unequal, whereas Mann–Whitney U tests were applied for non-normally distributed data. For experiments involving repeated measures over time, such as LTD time-course analyses, mixed-effects models with restricted maximum likelihood (REML) estimation were used, with Genotype, Cell type, or Age as fixed factors and individual neurons treated as random effects. When appropriate, post hoc comparisons were performed using Sidak's or Tukey's multiple-comparison tests. Paired-pulse ratio analyses were assessed using unpaired two-tailed t-tests. Data are

presented as mean ± s.e.m., and statistical significance was defined as $p < 0.05$. Exact p values, test statistics, degrees of freedom, and sample sizes are reported in the corresponding figure legends.

References

1. Dubois B*, et al.* Alzheimer Disease as a Clinical-Biological Construct-An International Working Group Recommendation. *JAMA Neurol* **81**, 1304-1311 (2024).
2. Migeot J*, et al.* Social exposome and brain health outcomes of dementia across Latin America. *Nat Commun* **16**, 8196 (2025).
3. Selkoe DJ, Hardy J. The amyloid hypothesis of Alzheimer's disease at 25 years. *EMBO Mol Med* **8**, 595-608 (2016).
4. Masters MC, Morris JC, Roe CM. "Noncognitive" symptoms of early Alzheimer disease: a longitudinal analysis. *Neurology* **84**, 617-622 (2015).
5. Shah J*, et al.* Predicting cognitive decline from neuropsychiatric symptoms and Alzheimer's disease biomarkers: A machine learning approach to a population-based data. *J Alzheimers Dis* **103**, 833-843 (2025).
6. Riffo-Lepe N*, et al.* Synaptic and synchronic impairments in subcortical brain regions associated with early non-cognitive dysfunction in Alzheimer's disease. *Neural Regen Res* **21**, 248-264 (2025).
7. Pensalfini A*, et al.* Intracellular amyloid and the neuronal origin of Alzheimer neuritic plaques. *Neurobiol Dis* **71**, 53-61 (2014).
8. Iulita MF*, et al.* Intracellular Abeta pathology and early cognitive impairments in a transgenic rat overexpressing human amyloid precursor protein: a multidimensional study. *Acta Neuropathol Commun* **2**, 61 (2014).
9. Wirths O*, et al.* Intraneuronal Abeta accumulation precedes plaque formation in beta-amyloid precursor protein and presenilin-1 double-transgenic mice. *Neurosci Lett* **306**, 116-120 (2001).
10. Ochiishi T*, et al.* New Alzheimer's disease model mouse specialized for analyzing the function and toxicity of intraneuronal Amyloid beta oligomers. *Sci Rep* **9**, 17368 (2019).
11. LaFerla FM, Green KN, Oddo S. Intracellular amyloid-beta in Alzheimer's disease. *Nat Rev Neurosci* **8**, 499-509 (2007).
12. Chang M*, et al.* Intercellular communication in the brain through a dendritic nanotubular network. *Science* **390**, eadr7403 (2025).
13. Alcantara-Gonzalez D, Kennedy M, Criscuolo C, Botterill J, Scharfman HE. Increased excitability of dentate gyrus mossy cells occurs early in life in the Tg2576 model of Alzheimer's disease. *Alzheimers Res Ther* **17**, 105 (2025).
14. Wu XR*, et al.* Amygdala neuronal dyshomeostasis via 5-HT receptors mediates mood and cognitive defects in Alzheimer's disease. *Aging Cell* **23**, e14187 (2024).
15. Kelly L*, et al.* Identification of intraneuronal amyloid beta oligomers in locus coeruleus neurons of Alzheimer's patients and their potential impact on inhibitory neurotransmitter receptors and neuronal excitability. *Neuropathol Appl Neurobiol* **47**, 488-505 (2021).
16. Cordella A*, et al.* Dopamine loss alters the hippocampus-nucleus accumbens synaptic transmission in the Tg2576 mouse model of Alzheimer's disease. *Neurobiol Dis* **116**, 142-154 (2018).
17. Russo SJ, Nestler EJ. The brain reward circuitry in mood disorders. *Nat Rev Neurosci* **14**, 609-625 (2013).

18. Floresco SB. The nucleus accumbens: an interface between cognition, emotion, and action. *Annu Rev Psychol* **66**, 25-52 (2015).
19. Contreras JA*, et al.* Functional connectivity among brain regions affected in Alzheimer's disease is associated with CSF TNF-alpha in APOE4 carriers. *Neurobiol Aging* **86**, 112-122 (2020).
20. Nie X*, et al.* Subregional Structural Alterations in Hippocampus and Nucleus Accumbens Correlate with the Clinical Impairment in Patients with Alzheimer's Disease Clinical Spectrum: Parallel Combining Volume and Vertex-Based Approach. *Front Neurol* **8**, 399 (2017).
21. Fernandez-Perez EJ*, et al.* Changes in neuronal excitability and synaptic transmission in nucleus accumbens in a transgenic Alzheimer's disease mouse model. *Sci Rep* **10**, 19606 (2020).
22. Armijo-Weingart L*, et al.* Loss of glycine receptors in the nucleus accumbens and ethanol reward in an Alzheimer s Disease mouse model. *Prog Neurobiol* **237**, 102616 (2024).
23. Vieitas-Gaspar N, Soares-Cunha C, Rodrigues AJ. From valence encoding to motivated behavior: A focus on the nucleus accumbens circuitry. *Neurosci Biobehav Rev* **172**, 106125 (2025).
24. Scaduto P*, et al.* Functional excitatory to inhibitory synaptic imbalance and loss of cognitive performance in people with Alzheimer's disease neuropathologic change. *Acta Neuropathol* **145**, 303-324 (2023).
25. Li G, Hsu LM, Wu Y, Bozoki AC, Shih YI, Yap PT. Revealing excitation-inhibition imbalance in Alzheimer's disease using multiscale neural model inversion of resting-state functional MRI. *Commun Med (Lond)* **5**, 17 (2025).
26. Kauer JA, Malenka RC. Synaptic plasticity and addiction. *Nat Rev Neurosci* **8**, 844-858 (2007).
27. Thomas MJ, Beurrier C, Bonci A, Malenka RC. Long-term depression in the nucleus accumbens: a neural correlate of behavioral sensitization to cocaine. *Nat Neurosci* **4**, 1217-1223 (2001).
28. Mango D, Ledonne A. Updates on the Physiopathology of Group I Metabotropic Glutamate Receptors (mGluRI)-Dependent Long-Term Depression. *Cells* **12**, (2023).
29. Luscher C, Huber KM. Group 1 mGluR-dependent synaptic long-term depression: mechanisms and implications for circuitry and disease. *Neuron* **65**, 445-459 (2010).
30. Turner BD, Kashima DT, Manz KM, Grueter CA, Grueter BA. Synaptic Plasticity in the Nucleus Accumbens: Lessons Learned from Experience. *ACS Chem Neurosci* **9**, 2114-2126 (2018).
31. Scheyer AF, Christian DT, Wolf ME, Tseng KY. Emergence of Endocytosis-Dependent mGlu1 LTD at Nucleus Accumbens Synapses After Withdrawal From Cocaine Self-Administration. *Front Synaptic Neurosci* **10**, 36 (2018).
32. Conrad KL*, et al.* Formation of accumbens GluR2-lacking AMPA receptors mediates incubation of cocaine craving. *Nature* **454**, 118-121 (2008).
33. Carr KD. Homeostatic regulation of reward via synaptic insertion of calcium-permeable AMPA receptors in nucleus accumbens. *Physiol Behav* **219**, 112850 (2020).
34. Ouyang J*, et al.* Food restriction induces synaptic incorporation of calcium-permeable AMPA receptors in nucleus accumbens. *Eur J Neurosci* **45**, 826-836 (2017).
35. McCutcheon JE, Loweth JA, Ford KA, Marinelli M, Wolf ME, Tseng KY. Group I mGluR activation reverses cocaine-induced accumulation of calcium-permeable AMPA receptors in nucleus accumbens synapses via a protein kinase C-dependent mechanism. *J Neurosci* **31**, 14536-14541 (2011).

36. Wong B, Zimbelman AR, Milovanovic M, Wolf ME, Stefanik MT. GluA2-lacking AMPA receptors in the nucleus accumbens core and shell contribute to the incubation of oxycodone craving in male rats. *Addict Biol* **27**, e13237 (2022).
37. Wolf ME, Tseng KY. Calcium-permeable AMPA receptors in the VTA and nucleus accumbens after cocaine exposure: when, how, and why? *Front Mol Neurosci* **5**, 72 (2012).
38. Henley JM, Wilkinson KA. Synaptic AMPA receptor composition in development, plasticity and disease. *Nat Rev Neurosci* **17**, 337-350 (2016).
39. Cull-Candy SG, Farrant M. Ca(2+) -permeable AMPA receptors and their auxiliary subunits in synaptic plasticity and disease. *J Physiol* **599**, 2655-2671 (2021).
40. Italia M, Scheggia D, DiLuca M, Gardoni F. What's in your plate?AMPA receptors modulation at the crossroads of homeostatic and hedonic eating. *Pharmacol Res* **217**, 107821 (2025).
41. Whitehead G*, et al.* Acute stress causes rapid synaptic insertion of Ca2+ -permeable AMPA receptors to facilitate long-term potentiation in the hippocampus. *Brain* **136**, 3753-3765 (2013).
42. Whitcomb DJ*, et al.* Intracellular oligomeric amyloid-beta rapidly regulates GluA1 subunit of AMPA receptor in the hippocampus. *Sci Rep* **5**, 10934 (2015).
43. Pilotto A*, et al.* Dopaminergic deficits along the spectrum of Alzheimer's disease. *Molecular Psychiatry*, (2025).
44. Storga D, Vrecko K, Birkmayer JG, Reibnegger G. Monoaminergic neurotransmitters, their precursors and metabolites in brains of Alzheimer patients. *Neurosci Lett* **203**, 29-32 (1996).
45. Nobili A*, et al.* Dopamine neuronal loss contributes to memory and reward dysfunction in a model of Alzheimer's disease. *Nat Commun* **8**, 14727 (2017).
46. Krashia P, Nobili A, D'Amelio M. Unifying Hypothesis of Dopamine Neuron Loss in Neurodegenerative Diseases: Focusing on Alzheimer's Disease. *Front Mol Neurosci* **12**, 123 (2019).
47. Baez S*, et al.* Moral Emotions and Their Brain Structural Correlates Across Neurodegenerative Disorders. *J Alzheimers Dis* **92**, 153-169 (2023).
48. Zufferey V, Gunten AV, Kherif F. Interactions between Personality, Depression, Anxiety and Cognition to Understand Early Stage of Alzheimer's Disease. *Curr Top Med Chem* **20**, 782-791 (2020).
49. Frank P*, et al.* Specific midlife depressive symptoms and long-term dementia risk: a 23-year UK prospective cohort study. *Lancet Psychiatry*, (2025).
50. Frisoni GB. Alzheimer disease: biomarker trajectories across stages of Alzheimer disease. *Nat Rev Neurol* **8**, 299-300 (2012).
51. Jeremic D, Jimenez-Diaz L, Navarro-Lopez JD. Past, present and future of therapeutic strategies against amyloid-beta peptides in Alzheimer's disease: a systematic review. *Ageing Res Rev* **72**, 101496 (2021).
52. Cline EN, Bicca MA, Viola KL, Klein WL. The Amyloid-beta Oligomer Hypothesis: Beginning of the Third Decade. *J Alzheimers Dis* **64**, S567-S610 (2018).
53. Daini E, Secco V, Liao W, Zoli M, Vilella A. A regional and cellular analysis of the early intracellular and extracellular accumulation of Abeta in the brain of 5XFAD mice. *Neurosci Lett* **754**, 135869 (2021).
54. Drummond E*, et al.* The amyloid plaque proteome in early onset Alzheimer's disease and Down syndrome. *Acta Neuropathol Commun* **10**, 53 (2022).
55. Belfiore R*, et al.* Temporal and regional progression of Alzheimer's disease-like pathology in 3xTg-AD mice. *Aging Cell* **18**, e12873 (2019).
56. Youmans KL*, et al.* Intraneuronal Abeta detection in 5xFAD mice by a new Abeta-specific antibody. *Mol Neurodegener* **7**, 8 (2012).

57. Zhong MZ, Peng T, Duarte ML, Wang M, Cai D. Updates on mouse models of Alzheimer's disease. *Mol Neurodegener* **19**, 23 (2024).
58. Hwang E-K, Wunsch AM, Wolf ME. Retinoic acid-mediated homeostatic plasticity drives cell type-specific CP-AMPAR accumulation in nucleus accumbens core and incubation of cocaine craving. *Molecular Psychiatry* **30**, 3175-3187 (2025).
59. Kawa AB, Hwang EK, Funke JR, Zhou H, Costa-Mattioli M, Wolf ME. Positive Allosteric Modulation of mGlu(1) Reverses Cocaine-Induced Behavioral and Synaptic Plasticity Through the Integrated Stress Response and Oligophrenin-1. *Biol Psychiatry* **92**, 871-879 (2022).
60. Valdivia G*, et al.* mGluR-dependent plasticity in rodent models of Alzheimer's disease. *Front Synaptic Neurosci* **15**, 1123294 (2023).
61. Gerlach M, Double K, Arzberger T, Leblhuber F, Tatschner T, Riederer P. Dopamine receptor agonists in current clinical use: comparative dopamine receptor binding profiles defined in the human striatum. *J Neural Transm (Vienna)* **110**, 1119-1127 (2003).
62. Richfield EK, Penney JB, Young AB. Anatomical and affinity state comparisons between dopamine D1 and D2 receptors in the rat central nervous system. *Neuroscience* **30**, 767-777 (1989).
63. Beaulieu JM, Gainetdinov RR. The physiology, signaling, and pharmacology of dopamine receptors. *Pharmacol Rev* **63**, 182-217 (2011).
64. Aguado C*, et al.* Resilience to structural and molecular changes in excitatory synapses in the hippocampus contributes to cognitive function recovery in Tg2576 mice. *Neural Regen Res* **19**, 2068-2074 (2024).
65. Guo C*, et al.* Amyloid-beta oligomers in the nucleus accumbens decrease motivation via insertion of calcium-permeable AMPA receptors. *Mol Psychiatry* **27**, 2146-2157 (2022).
66. Peterson BM, Martinez LA, Meisel RL, Mermelstein PG. Estradiol impacts the endocannabinoid system in female rats to influence behavioral and structural responses to cocaine. *Neuropharmacology* **110**, 118-124 (2016).
67. Fernandez-Perez EJ*, et al.* Synaptic dysregulation and hyperexcitability induced by intracellular amyloid beta oligomers. *Aging Cell* **20**, e13455 (2021).
68. Saavedra-Sieyes P, Meza I, Riffo-Lepe N, San Martin L, Gonzalez-SanMiguel J, Aguayo LG. Alterations in neuronal excitability and AMPA-mediated neurotransmission in an APP/PS1 neuronal culture model derived from nucleus accumbens. *J Alzheimers Dis*, 13872877251378468 (2025).
69. Jankowsky JL, Slunt HH, Ratovitski T, Jenkins NA, Copeland NG, Borchelt DR. Co-expression of multiple transgenes in mouse CNS: a comparison of strategies. *Biomol Eng* **17**, 157-165 (2001).
70. Ade KK, Wan Y, Chen M, Gloss B, Calakos N. An Improved BAC Transgenic Fluorescent Reporter Line for Sensitive and Specific Identification of Striatonigral Medium Spiny Neurons. *Front Syst Neurosci* **5**, 32 (2011).

Data availability

The data supporting the findings of this study are available from the corresponding author upon reasonable request.

Acknowledgements

We thank Laurie Aguayo, Helena Zambrano, and Ailine Riquelme for technical assistance, as well as Jocelyn González and Ixia Cid for support during experimental

procedures. We also acknowledge Carolina Benítez (CREAV-UDEC) and Claudia Ramírez for veterinary assistance. We thank Lauren Aguayo and Mauricio Avendaño Valenzuela (Universidad de Concepción, Chile) for assistance with language editing. This work was supported by ANID Fondecyt Regular grant 1221080 (L.G.A.), a PhD fellowship from ANID (21202521) awarded to N.R.L., and NIH grant R01AA025718 (L.G.A.).

Author contributions

N.R.L.: Conceptualization, methodology, investigation, formal analysis, visualization, writing - original draft, writing - review & editing. J.G.S.: Investigation, formal analysis, writing & review. I.M.: Investigation, formal analysis, writing & review. L.A.W.: Investigation, formal analysis, writing & review. P.S.S.: Investigation, formal analysis, writing & editing. A.S.: Methodology, supervision, writing & review. L.S.M.: Conceptualization, supervision, writing & review. L.G.A.*: Conceptualization, methodology, supervision, writing - review & editing, project administration, funding acquisition.

Competing interests

The authors declare no competing interests.

Additional Information

Correspondence and requests for materials should be addressed to Luis G. Aguayo.